JGS
Journal of the Geological Society

Research article

Published Online First

https://doi.org/10.1144/jgs2021-018

Geochemistry of macrofossil, bulk rock and secondary calcite in the Early Jurassic strata of the Llanbedr (Mochras Farm) drill core, Cardigan Bay Basin, Wales, UK

Clemens V. Ullmann[1,2]*, Dominika Szűcs[2], Mengjie Jiang[2], Alexander J.L. Hudson[2] and Stephen P. Hesselbo[2]

[1] University of Oxford, Department of Earth Sciences, 3 South Parks Road, Oxford OX1 3AN, UK
[2] University of Exeter, Camborne School of Mines, Penryn Campus, Treliever Road, Penryn TR10 9FE, Cornwall, UK
CVU, 0000-0002-5865-7289; DS, 0000-0001-6061-2082
* Correspondence: c.ullmann@exeter.ac.uk

Abstract: The Llanbedr (Mochras Farm) core (Wales, UK) yielded a >1300 m long mudrock sequence that has excellent potential for establishing an integrated stratigraphic scheme for the entire Early Jurassic Epoch. Lithological variations in the core are predominantly driven by hierarchical changes in the carbonate content. These changes also dominate – or may impact upon – many geochemical and physical properties of the core. The bulk carbonate C isotope record displays systematic fluctuations, the largest of which correspond to previously identified phases of environmental perturbation. The magnitudes of negative C isotope excursions in carbonate are inflated compared with equivalents previously described elsewhere as a result of diagenesis and the concomitant loss of primary carbonate. The marine macrofossil record of Mochras reveals biological and isotopic patterns that are generally comparable with other UK basins. Potentially significant differences between the Cleveland and Cardigan Bay basins are observed in the Pliensbachian and Toarcian fossils. This different expression may be related to different habitat structures or palaeoceanographic and water depth differences between these basins. Minima in macrofossil $\delta^{18}O$ values generally coincide with peaks in macrofossil wood abundance and sea-level lowstands inferred from sequence stratigraphic interpretation of other UK sections. This relationship suggests a possible relative sea-level control on the observed O isotope records and sediment provenance.

Supplementary material: Analytical data for the Mochras core are available at https://doi.org/10.6084/m9.figshare.c.5463508

Received 5 February 2021; **revised** 30 May 2021; **accepted** 10 June 2021

Integrated stratigraphic schemes for extended intervals of geological time are of great importance for understanding palaeoenvironments. They allow a unified view of multiple proxies for palaeoenvironmental and stratigraphic conditions, avoiding correlation errors and age uncertainties unavoidable in compilations of composite stratigraphic records. Integrated stratigraphic schemes also allow for high-accuracy correlations to other sedimentary successions, giving a global view of palaeoenvironmental conditions and their changes through time. Such integrated stratigraphic schemes are particularly important in the Early Jurassic, for which comparatively large uncertainties in the numerical ages of stage boundaries, durations of ammonite biozones and problems with long-range correlations still exist (Hesselbo *et al.* 2020*a*).

The Llanbedr (Mochras Farm) borehole was drilled onshore in the Cardigan Bay Basin (Wales, UK) in 1967–69 (history summarized in Copestake and Johnson 2014). A thick Mesozoic sequence, including 1300 m of Early Jurassic sedimentary strata, was recovered below a 600 m thick Cenozoic cover (Wood and Woodland 1968; Woodland 1971). All boreal ammonite zones of the Early Jurassic, except the earliest Hettangian *tilmanni* Zone, were shown to be present at the site (Woodland 1971; Copestake and Johnson 2014), indicating that breaks in sedimentation and faults, if present, did not cause major stratigraphic gaps.

Updated ammonite and foram biostratigraphies are already available for the core (Copestake and Johnson 2014). Low-resolution carbonate and organic matter C isotope chemostratigraphies have also been published (Jenkyns *et al.* 2002; Katz *et al.* 2005; van de Schootbrugge *et al.* 2005*a*). More recently, a higher resolution organic matter C isotope chemostratigraphy based on 1760 samples (Xu *et al.* 2018*a*; Storm *et al.* 2020) and Toarcian magnetostratigraphy (Xu *et al.* 2018*b*) have been established. The clay fraction of the middle Sinemurian to upper Pliensbachian part of the core has also been studied and systematic changes in the relative clay abundance have been linked to shifting climate conditions (Deconinck *et al.* 2019; Munier *et al.* 2020). The Pliensbachian section of the core has been the subject of cyclostratigraphic interpretation from time series of the major element content, the cyclic character of which is governed principally by regular fluctuations in carbonate content (Ruhl *et al.* 2016).

Despite its importance for cyclo-, bio- and chemostratigraphy, the calcite fraction of the Mochras core has not yet been studied petrographically or geochemically in any detail. Carbonate C isotope chemostratigraphy at Mochras is limited to the dataset of Katz *et al.* (2005) at *c.* 8 m resolution and 71 analyses for the Toarcian and upper Pliensbachian presented by Jenkyns *et al.* (2002). Geochemical assessments of clearly diagenetic calcite, such as veins and slickensides, as well as of macrofossil calcite, are lacking.

To better understand the nature of the carbonate of the Mochras core and the environmental signatures encoded therein, we undertook a detailed study of the various carbonate phases present at Mochras. We report here C and O isotope data and the carbonate content of 961 bulk rock samples, and C and O isotope and element/Ca ratios for 243 samples of diagenetic phases and 335 samples of macrofossil calcite. These data are supplemented by

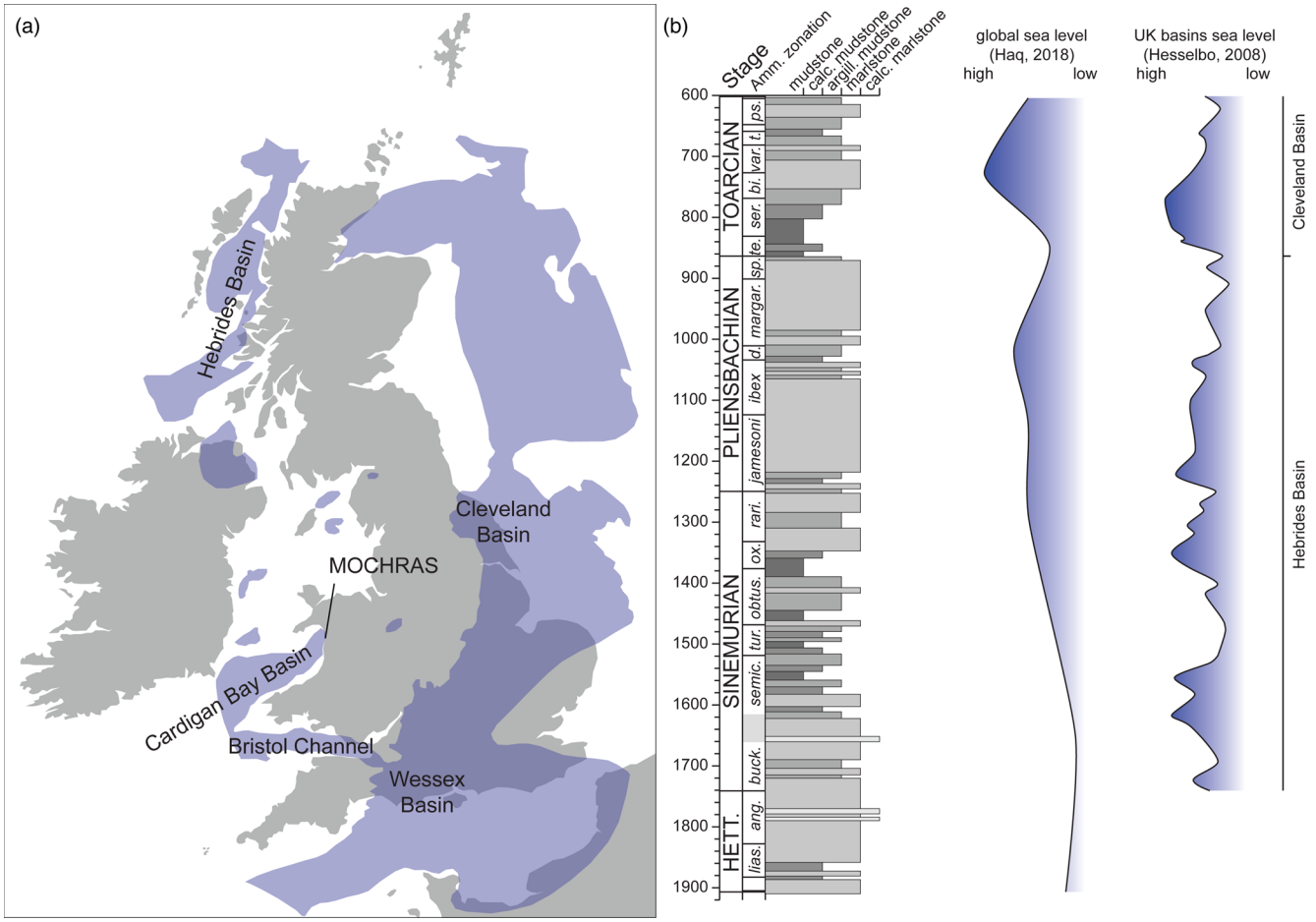

Fig. 1. (**a**) Jurassic strata onshore and offshore UK and Ireland, including the location of the Mochras core. Map modified from Barron *et al.* (2012). (**b**) Simplified lithological log of the Mochras core, including sea-level reconstructions for global sea-level redrawn from Haq (2018) and sea-level reconstructions for the UK redrawn from Hesselbo (2008).

observations of stratigraphic trends in fossil preservation and petrographic observations of diagenetic sequences.

Geological background

The Llanbedr (Mochras Farm) core was drilled onshore within the Cardigan Bay Basin (Fig. 1), a broadly NE–SW-oriented half-graben structure bounded to the SE by the Bala fault system (Dobson and Whittington 1987; Tappin *et al.* 1994). The Mochras fault, which is a major normal fault closely adjacent to the borehole site, may have created subsidence at that location, but the timing of its activity is currently uncertain. Although some researchers regard this north–south-striking and west-dipping fault system lying *c.* 1 km to the east as solely Cenozoic in origin (e.g. Dobson and Whittington 1987), others have interpreted the structure as synsedimentary (e.g. Xu *et al.* 2018*a*).

The Lower Jurassic strata at Mochras were deposited in a fully marine depositional setting located in close proximity to the Welsh Massif (Deconinck *et al.* 2019), which at the time consisted of a series of relatively low-relief islands formed from the predominantly Caledonian basement and localized Carboniferous sedimentary strata (Cope *et al.* 1992; Tappin *et al.* 1994). Deposition in the Cardigan Bay Basin was interrupted by uplift, principally in the Middle Jurassic and Early Cretaceous (Tappin *et al.* 1994; Holford *et al.* 2005), which caused erosion and the development of an important hiatus at Mochras. The uppermost Toarcian at Mochras is unconformably overlain by Oligocene–Miocene continental deposits as a result of extensional activity on the Mochras fault (Wood and Woodland 1968; Dobson and Whittington 1987).

Lower Jurassic siliciclastic deposits at Mochras are believed to be derived from Caledonian and Variscan sources (Munier *et al.* 2020). Based on locally abundant terrestrial plant matter, the siliciclastic fraction has been linked to sources further afield than Wales, including Cornubia, the London–Brabant Massif and the Irish Massif (van de Schootbrugge *et al.* 2005*a*). Although a detailed assessment of nannofossils in the core is still outstanding, the carbonate of the core constitutes a mixture of shallow-marine platform-derived carbonate and pelagic carbonate (van de Schootbrugge *et al.* 2005*b*), more or less altered by recrystallization and reprecipitation, in line with other Jurassic basins in the same region (e.g. Weedon 1986; Sheppard *et al.* 2006; Ruhl *et al.* 2016; Weedon *et al.* 2018).

Materials and methods

The drill core and related samples are stored at the National Geological Repository of the British Geological Survey, Keyworth, UK. About half of the originally nearly fully recovered core was broken up soon after recovery. Consequently, for the Jurassic part of the core, only the archive half from 1282 to 601 m depth, corresponding to the uppermost Sinemurian to top Toarcian stages, is still present with the stratigraphic context preserved. Short disjointed intervals of core further down in the succession exist, but provide little opportunity for generating coherent records. However, nearly 7800 discrete fossil specimens registered with a core depth of one-inch precision, and aggregate bags of *c.* 500 g of core fragments, each corresponding to *c.* 1.4 m of cored interval, are also archived. These materials constitute valuable resources from

which to construct multiproxy datasets and an integrated stratigraphy for the entire Early Jurassic of the Mochras core at high resolution.

Bulk rock, vein calcite, slickenside and macrofossil specimens were selected from aggregate bags of the Mochras core and supplemented with a small number of fossil specimens loaned from the registered specimen collection. About 50 mg of bulk rock or *c.* 10 mg of diagenetic materials were extracted from selected rock specimens using a hand-held drill with a diamond-coated steel bit. For the macrofossils, fragmentary rock material from the aggregate bags was checked for the presence of macrofossil material of sufficient size for analysis and initial preservation checks were carried out by naked eye and hand lens. Only specimens passing general preservation criteria, such as amber–brown transparent calcite for belemnite rostra and silky reflection of the fibrous secondary shell layers of brachiopods, were selected for analytical work.

A few milligrams of calcite powder were extracted from belemnite rostra using a hand-held drill. We preferentially targeted translucent material, devoid of any clear cracks and secondary mineral formation, intermediate between the apical line and rims in the stem region of the belemnite rostra (Saelen and Karstang 1989; McArthur *et al.* 2000; Ullmann *et al.* 2015). For bivalve and brachiopod fossils, similar amounts of shell material were extracted from pre-cleaned surfaces using a stainless-steel scalpel or preparation needles (Korte and Hesselbo 2011). In the case of brachiopods, material was only taken from fibrous secondary shell layers.

For the depth interval from 1210 to 1745 m, a total of 1553 analyses of the Ca content as a proxy for the carbonate content were also conducted on bulk rock from the remaining archive core and registered specimens using a portable X-ray fluorescence (p-XRF) spectrometer.

Petrographic observations

Samples for petrographic observation were prepared from oriented samples cut from the Pliensbachian and uppermost Sinemurian archive material of the Mochras core. Thin sections were mechanically polished at the University of Oxford using minimal water during grinding and polishing to prevent the loss of clay. The sections were first studied using a petrographic microscope and then coated with a *c.* 25 nm thick layer of carbon. Detailed high-resolution observations were then made at the University of Exeter, Penryn Campus, using a FEI Quantax FEG 650 scanning electron microscope equipped with an energy-dispersive spectrometer with two Bruker XFlash series 6|30 SDD detectors. For observations in the high-vacuum mode, the accelerator voltage was set at 15 kV, with a working distance of 13 mm and a spot size of 3.0 µm.

Stable C and O isotope ratio determination

A total of 1544 analyses of $\delta^{13}C$ and $\delta^{18}O$ were carried out for the present study and supplemented by 231 bulk rock values compiled from the literature (Jenkyns *et al.* 2002; Katz *et al.* 2005).

All the bulk rock samples and the majority of the vein, slickenside and fossil calcite samples were analysed at the University of Exeter, Penryn Campus, using a Sercon 20-22 gas source isotope ratio mass spectrometer in a continuous flow setup. The analytical methods were analogous to those of Ullmann *et al.* (2020) and are explained only in brief. Fossil samples of *c.* 500 µg or bulk samples with an equivalent weight of 500 µg calcite were weighed into borosilicate vials at 1 µg precision. This enabled the precise carbonate content to be calculated via the calibration of signal yields of in-house standards. Samples and in-house standards CAR (Carrara Marble, $\delta^{13}C_{carb} = +2.10‰$ V-PDB; $\delta^{18}O_{carb} = -2.03‰$ V-PDB) and NCA (Namibian carbonatite, $\delta^{13}C_{carb} = -5.63‰$ V-PDB; $\delta^{18}O_{carb} = -21.90‰$ V-PDB) were flushed with He for 80 s and reacted with nominally anhydrous phosphoric acid (103%) at 70°C. Instrumental drift and analytical bias were corrected using the two in-house standards yielding a reproducibility (two standard deviations; 2 SD) of 0.07‰ for $\delta^{13}C_{carb}$ and 0.16‰ for $\delta^{18}O_{carb}$ ($n = 390$). The carbonate content of NCA (2 SD) was 97.1 ± 1.4% ($n = 132$).

A total of 71 fossil samples and nine samples of diagenetic calcite were measured at the University of Copenhagen, using either an IsoPrime gas source isotope ratio mass spectrometer in a continuous flow setup following the routines described in Ullmann *et al.* (2013) or a Delta gas source isotope ratio mass spectrometer coupled with a Kiel IV device following the procedures outlined in Ullmann *et al.* (2017). For the IsoPrime spectrometer, the data were corrected using the in-house standard LEO (Carrara Marble, $\delta^{13}C_{carb} = +1.96‰$ V-PDB; $\delta^{18}O_{carb} = -1.93‰$ V-PDB). Repeat measurements ($n = 14$) for this standard gave a reproducibility (2 SD) of 0.10‰ for $\delta^{13}C_{carb}$ and 0.15‰ for $\delta^{18}O_{carb}$. For the Delta gas source isotope ratio mass spectrometer, the data were measured alongside the international standards NBS-18 and NBS-19 and the instrumental bias was corrected with a two-point calibration using the average results for these standards. The accuracy of the measurements was controlled via multiple measurements of the in-house standard LM (Laaser Marble, $\delta^{13}C_{carb} = +1.51‰$ V-PDB; $\delta^{18}O_{carb} = -5.17‰$ V-PDB), which gave averages ($n = 9$; 2 SD) of +1.51 ± 0.03‰ for $\delta^{13}C_{carb}$ and −5.15 ± 0.09‰ for $\delta^{18}O_{carb}$.

Element/Ca ratios

Element/Ca ratios for most of the fossils and vein material were measured using an Agilent 5110 VDV inductively coupled plasma optical emission spectrometer at the University of Exeter, Penryn Campus, following the methods outlined in detail in Ullmann *et al.* (2020). In brief, samples of a target weight of 500 µg were weighed at 1 µg precision, transferred into 15 mL centrifuge tubes and dissolved with 2% *V*/*V* nitric acid at a ratio of 1.5 mL per 100 µg to achieve a nominal Ca concentration of 25 µg g^{-1} in solution. Signals were quantified using a four-point calibration, including three matrix-matched calibration solutions made from certified single-element standards and a blank solution. The internal consistency of the analyses was checked using a quality control solution made from the same certified single-element standards. The reproducibility of the analyses was controlled by repeat measurements of international standards JLs-1 and AK, giving a reproducibility (2 SD) of 1.1% or better for element/Ca ratios exceeding the quantification limits >100 times. Typical quantification limits of the measurements equate to 0.02 mmol mol^{-1} for Mg/Ca, 0.0004 mmol mol^{-1} for Sr/Ca, 0.006 mmol mol^{-1} for Mn/Ca, 0.02 mmol mol^{-1} for Fe/Ca, 0.5 mmol mol^{-1} for S/Ca and 1 mmol mol^{-1} for P/Ca. The reproducibility (2 SD) of element/Ca ratios <100 times the quantification limit was better than 0.03 mmol mol^{-1} for Mg/Ca, 0.004 mmol mol^{-1} for Sr/Ca, 0.002 mmol mol^{-1} for Mn/Ca, 0.07 mmol mol^{-1} for Fe/Ca, 0.3 mmol mol^{-1} for S/Ca and 0.12 mmol mol^{-1} for P/Ca ratios.

Element/Ca ratios for samples analysed in Copenhagen were measured following the routines described in Ullmann *et al.* (2017) using an Optima 7000 DV inductively coupled plasma optical emission spectrometer. The average element/Ca ratios and reproducibility (2 SD) for the international standard JLs-1 were indistinguishable from those reported in Ullmann *et al.* (2017), apart from a slightly higher uncertainty of 0.02 mmol mol^{-1} for Mn/Ca. These values suggest that the analytical uncertainty of the measurements (2 SD) was better than 2.5% for Mg/Ca and Sr/Ca. For Fe/Ca, the uncertainty was 0.04 mmol mol^{-1} or 4% (two relative standard deviations; 2 RSD) and 0.02 mmol mol^{-1} or 2% (2 RSD) for Mn/Ca, depending on which was the larger value.

Results

Carbonate content

Carbonate concentration data from the Mochras core have previously been generated using widely differing techniques, with the largest quantity of data deriving from p-XRF measurements. To calibrate for the instrumental bias of this semi-quantitative technique, we binned these data into 5 m intervals and matched them with published Rock–Eval data similarly averaged over 5 m (Fig. 2). Instrumental bias was then accounted for by applying the resulting linear correction functions to all the p-XRF data. Separate correlation lines were constructed for the Toarcian and Pliensbachian data because they were generated with different p-XRF devices and under different analytical conditions.

The resulting compilation of >7700 samples, including >2500 newly measured carbonate content estimates, is presented in Figure 3. The density of data is highest where intact archive core material is preserved and decreases towards the bottom of the core, with very sparse data around depths of 1650–1850 m. Averages and the variability in carbonate content for the Hettangian and Sinemurian part of the core are therefore generally not very robust and only the coarse features are reliable. The carbonate content of the sedimentary strata in the Mochras core, however, does show systematic long-term fluctuations, which are consistent across multiple analytical techniques, even where only a few analyses have been made (Fig. 3).

The Hettangian part of the core is characterized by a substantial upwards reduction in carbonate content from about 60 wt.% in the *planorbis* Zone to about 25% in the lower part of the *liasicus* Zone. The carbonate content then increases upwards and becomes more variable up to about the Hettangian–Sinemurian boundary (1741 m), where a long-term decline in carbonate content commences. A local minimum in carbonate content is registered around the transition from the upper Sinemurian *obtusum* to *oxynotum* Zones, where values <10 wt.% are common. Above this minimum, the carbonate content increases into the lower Pliensbachian *jamesoni* Zone, briefly interrupted by a narrow, carbonate-lean interval just above the Sinemurian–Pliensbachian boundary. The Pliensbachian is then characterized by a slight reduction in carbonate content up to the *davoei* Zone, followed by an increase into the upper part of the *margaritatus* Zone. Above this optimum, the carbonate content shows a sustained decrease, with a narrow drop to very low values around the Pliensbachian–Toarcian boundary. Carbonate contents continue to fall until the lowest values are recorded in the lower Toarcian *serpentinum* Zone, where carbonate contents are typically <10 wt.%. Carbonate concentrations then recover to *c.* 30–40 wt.% for the remaining Toarcian, with a brief interval of slightly lower values for the *thouarsense* and *dispansum* Zones.

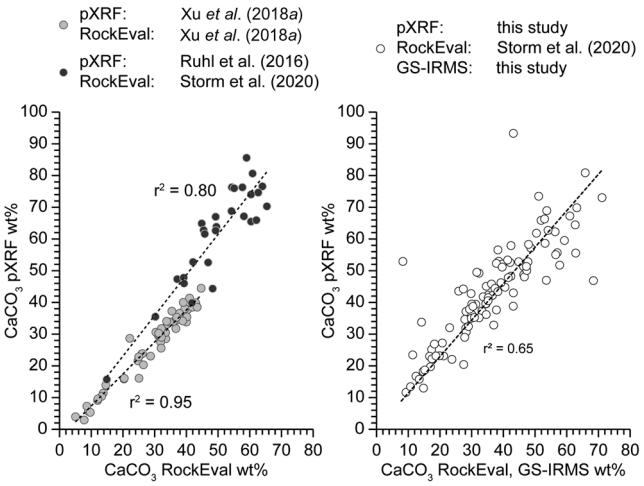

Fig. 2. Correlation of published $CaCO_3$ estimates derived from portable X-ray fluorescence (p-XRF) data (Ca × 2.5) v. estimates from Rock–Eval (mineral C × 25/3) (left-hand panel) and our newly analysed p-XRF data (right-hand panel). Data were binned in 5 m intervals to allow for a more robust comparison of different techniques. The vertical intercept for the Pliensbachian data from 860 to 1000 m depth (Ruhl *et al.* 2016; Storm *et al.* 2020) was set to the same as that observed for the dataset from Xu *et al.* (2018*a*). Correlation for the Pliensbachian was limited to this depth interval because the more widely spaced Rock–Eval measurements at greater depths result in much less robust averages against which to compare the XRF data.

Carbonate components

The carbonate constituents of the Mochras core are mostly hard to differentiate macroscopically. The remaining core is dominated by about 1 m thick couplets of bioturbated, comparatively carbonate-lean and carbonate-rich sediments, superimposed on long-term fluctuations in the overall carbonate content that are easily visible by changes in the lightness of the rock (Fig. 4).

The presence of calcite nodules can only be established in the uppermost Pliensbachian part of the core. Siderite, conspicuous as a result of its red weathering colour, occurs in a dispersed form, thin bands and also nodules, most prominently in the lower Toarcian part of the core (Fig. 4a; see Xu *et al.* 2018*a* for detailed observations). Isolated occurrences of siderite nodules have also been observed in the Sinemurian part of the core around the *obtusum* and *oxynotum* Zones – for example, specimen SSK78968 at a depth of 1386 m (Fig. 5c).

Medium- to coarse-grained calcite veins, partly with cavernous centres and calcitic slickensides, are common in the middle and upper Toarcian and in the *margaritatus* Zone of the Pliensbachian, where the veins can be several centimetres wide and can sometimes be traced for more than half a metre through the core sections (Fig. 4). By contrast, veins are virtually absent from the Hettangian and Sinemurian parts of the core and the slickensides, despite being present, are mostly devoid of carbonate accumulations. A microscopic study of the coarse-grained veins reveals the presence of minor amounts of celestine ($SrSO_4$), typically close to the vein margins, where it presents an interface with the sedimentary matrix (e.g. specimen SSK74581 at 991 m depth; Fig. 6b). In some instances, partial replacement of celestine by calcite is observed (e.g. specimen SSK74588 at 1016 m depth; Fig. 6).

Petrographic observations using scanning electron microscopy show the close association of celestine with smaller amounts of barite (Fig. 7a). More dispersed occurrences and pockets with common framboidal pyrite, partially euhedral carbonate minerals and bioclasts, kerogen and detrital material are also seen (Fig. 7b). Framboidal, subhedral and euhedral pyrite is often observed in association with macrofossils, both organic (plant remains) and shell material, where it occurs in cavities and replaces part of the original structure (Fig. 7c, d). Published X-ray diffraction measurements of Toarcian strata have yielded 0–4% Fe-dolomite with an average of 2% ($n = 36$) and no apparent co-variation with the calcite content (Xu *et al.* 2018*a*). Dolomite is ubiquitously observed under the scanning electron microscope, typically as idiomorphic crystals of tens of micrometres diameter, usually showing more Ca- or Fe-rich later overgrowths and sometimes multiple zoned rims (Fig. 7e, f).

Fossil abundance

The Mochras core is very rich in fossils, with a total of nearly 7800 registered specimens, most of which are carbonate shells, particularly ammonites (Fig. 8). A large number of macrofossil wood specimens are also recorded in the Mochras core, the vast

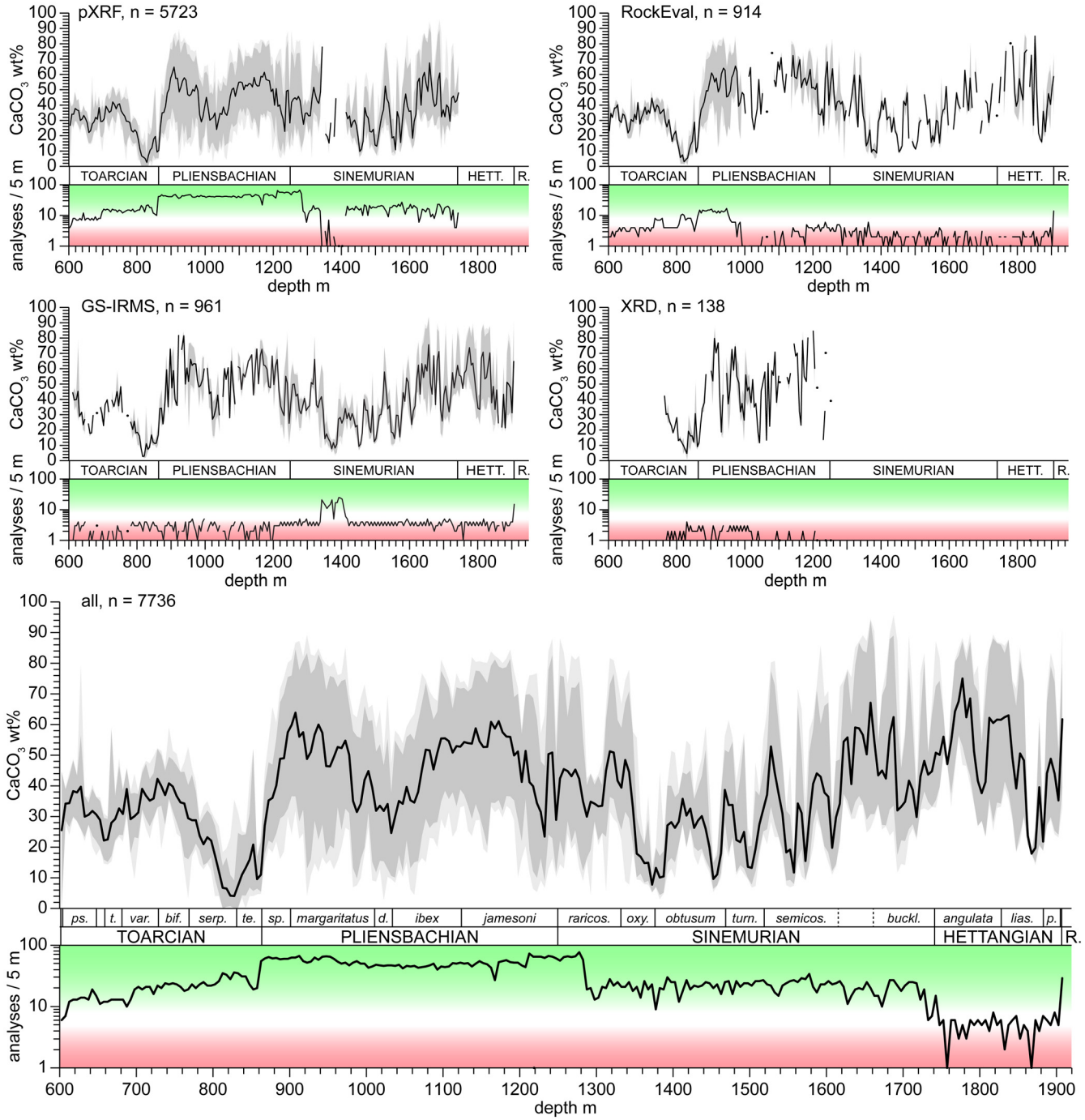

Fig. 3. Carbonate concentrations averaged for 5 m bins in Mochras bulk rock samples, split according to different analytical techniques and combined into a single compilation. The black lines indicate the average, the medium grey bands the 5–95 percentile range and the pale grey bands the absolute range of the observed values. The number of analyses for each 5 m bin, indicating the robustness of the computed averages, is shown in the lowest panel. The ammonite biozonation scheme is taken from Page in Copestake and Johnson (2014). Data coverage is highest in the Pliensbachian part of the core and becomes sparse from *c.* 1750 m to the base of the Jurassic. The data, where not generated for the present study, were taken from Ruhl *et al.* (2016); Xu *et al.* (2018*a*); Deconinck *et al.* (2019) and Storm *et al.* (2020).

majority of which are found in the Pliensbachian and Toarcian part (Fig. 8).

The most detailed record for any fossil group in the Mochras material at present is for the ammonites, which have been studied for biostratigraphic purposes and identified to species level in many cases. Ammonites are particularly common in the Toarcian part of the core, where, on average, four ammonites have been registered for each metre of core. Ammonite abundances are typically lower and more variable in the lower part of the core, averaging close to one ammonite per metre of core for the Hettangian, Sinemurian and Pliensbachian. Brief intervals similarly rich in ammonites to the Toarcian occur in the Sinemurian *semicostatum* Zone and the Hettangian *planorbis* Zone. A smaller core diameter stepping down from *c.* 110 mm diameter in the Toarcian and Pliensbachian to *c.* 90 mm at 1182 m depth (Pliensbachian *jamesoni* Zone down to the upper Triassic) may be partially responsible for this reduction in ammonite finds. However, the preservation of the archive core as thirds rather than half-core from 1182 m downwards indicates that this reduction in diameter was counteracted by breaking up larger amounts of core for fossil assessment. The four-fold decrease in

Fig. 4. Photographs of archive core sections with the section tops facing to the left. (**a**) Occurrence of siderite nodules in the lower Toarcian. Elevated Fe levels are visible as red surface staining of the aged archive core. (**b**) Calcite nodules in the upper Pliensbachian. Light, *c.* 8 cm-sized nodules are visible in the middle and lower parts of the core section. (**c**) Centimetre thick calcite veins in the upper Pliensbachian. (**d**) Typical dark–pale alternation on a metre scale in the lower Pliensbachian.

ammonite abundance can therefore not be explained by the reduced availability of material.

Belemnites, bivalves and brachiopods were collected from the reserve bag collection as part of this study. The material deemed suitable for geochemical investigations gives a broad guidance on the distribution of these different faunal groups in the core. The stratigraphically lowest fragment of a belemnite rostrum detected in the reserve bag material comes from a depth of *c.* 1585 m (lower *semicostatum* Zone) and occurrences are sparse below the upper Sinemurian (Fig. 8). A particularly belemnite-rich interval is in the upper *margaritatus* and *spinatum* Zones of the upper Pliensbachian. No belemnite is observed at the Pliensbachian–Toarcian boundary nor in the subsequent *c.* 15 m; they are again absent through most of the interval characterized by the negative C isotope excursion of the Toarcian oceanic anoxic event (T-OAE).

Large thick-shelled bivalves with visually good preservation are particularly abundant in the Hettangian and Sinemurian part of the core, whereas brachiopods are particularly abundant in the upper Sinemurian and upper Pliensbachian strata.

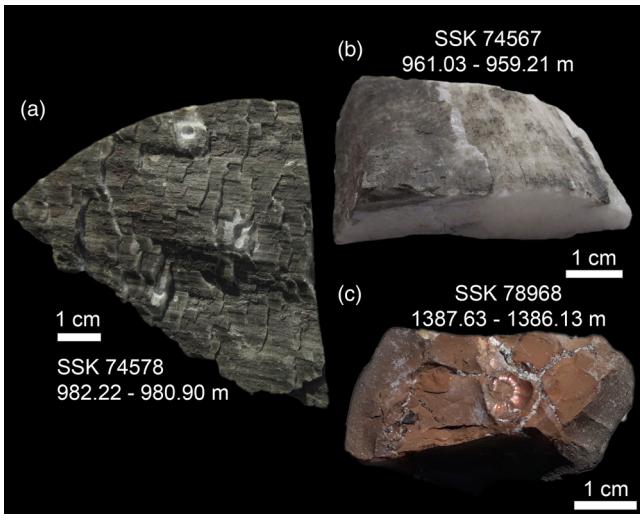

Fig. 5. Macroscopic diagenetic phases in the Mochras core. (**a**) Slickenside from the Pliensbachian *margaritatus* Zone. (**b**) Coarse-grained calcite vein from the *margaritatus* Zone. (**c**) Septarian siderite concretion with celestine crack fills and aragonitic ammonite as a possible nucleus from the Sinemurian *obtusum* Zone.

Fossil preservation

Fossil preservation in the Mochras core is optically very good. Ammonites with iridescent nacre are observed from the lowermost Hettangian to the lowermost Pliensbachian (*c.* 1210 m depth) and some fossil shells preserving non-iridescent aragonite are found above this level. Brachiopods often macroscopically show a silky reflection of their fibrous secondary shell layer. Belemnite rostra, where they are large enough, show semi-transparent, dark amber-coloured calcite, even though they tend to be strongly fractured, probably as a consequence of drilling disturbance.

Chemical preservation indices for the fossils indicate that the fossil material, on average, has retained most of its original composition and the palaeoenvironmental information is largely preserved. Of 171 analysed belemnite samples, 151 showed Mn/Ca ratios <0.05 mmol mol^{-1} and 150 showed Sr/Ca ratios >1.3 mmol mol^{-1}; 103 of 124 bivalve samples and 27 of 35 brachiopod samples had Mn/Ca ratios <0.3 mmol mol^{-1}.

Carbonate C and O isotope ratios

Bulk rock

Bulk carbonate C isotope data show a consistent pattern with little high-frequency noise (Fig. 8). A total of 95% of the data ($n = 1190$) fall in the range −2.6 to +3.2‰ V-PDB (median 1.2‰ V-PDB) and a total range of −8.9 to +4.1‰ V-PDB is observed. Broadly, C isotope ratios show an overall increase from the lowermost Jurassic, with values near +1.0‰ V-PDB, to the upper Pliensbachian, reaching values of *c.* +3.6‰ V-PDB at a depth of 960 m

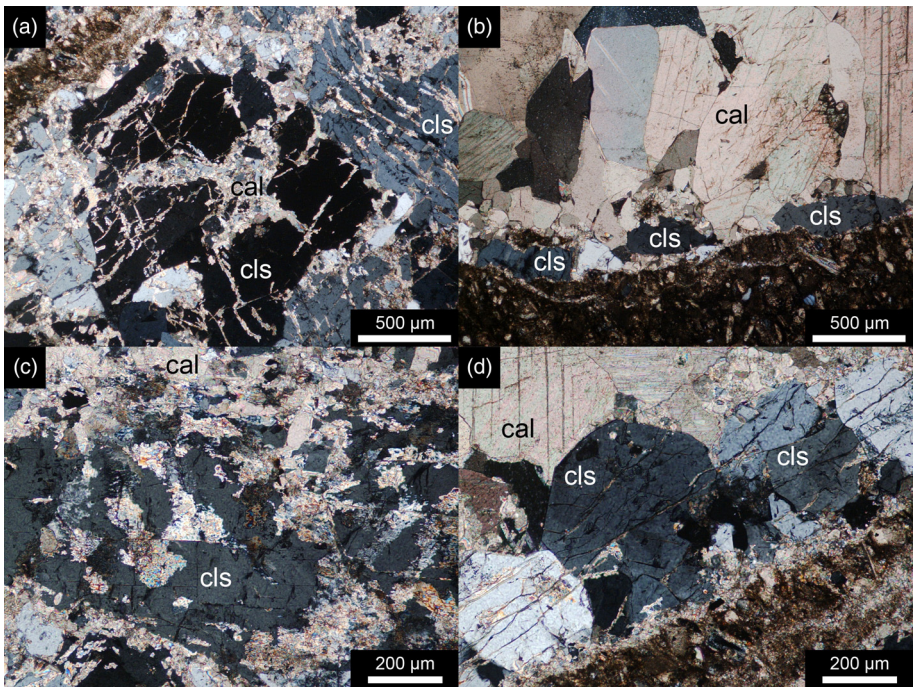

Fig. 6. Occurrence of celestine (cls) in calcite (cal) veins from the upper Pliensbachian (**a**, **c**, **d**) *davoei* Zone (SSK74588, 1016 m) and (**b**) *margaritatus* Zone (SSK74581, 991 m). Celestine is typically found on the edges of veins and is partially replaced by calcite. Three inductively coupled plasma optical emission spectrometry analyses of specimen SSK74588 yielded a distinctly reduced $CaCO_3$ content (21 and 34%) in two samples and a pure calcite sample with an elevated Sr/Ca ratio of 3.3 mmol mol^{-1} without a correspondingly high S/Ca ratio (see Supplementary data), suggesting the incorporation of Sr from consumed celestine into the vein calcite.

(*margaritatus* Zone). Values then decrease again towards the top Toarcian to near +1.7‰ V-PDB. A series of negative C isotope excursions is observed superimposed on this broader pattern. Particularly negative $\delta^{13}C_{carb}$ values are measured in intervals with a reduced carbonate content in the lower Hettangian, upper Sinemurian, at the Sinemurian–Pliensbachian boundary, in the middle Pliensbachian, at the Pliensbachian–Toarcian boundary and in the early Toarcian. The most pronounced of these negative excursions are found in the Sinemurian *obtusum* and *oxynotum* Zones and the Toarcian *serpentinum* Zone, where carbonate contents are often <10 wt.% (Fig. 9). In addition to the co-occurrence of negative $\delta^{13}C_{carb}$ values with low carbonate contents, bulk carbonate from the uppermost Triassic strata is depleted in $^{13}C_{carb}$ despite a moderate carbonate content of *c.* 60 wt.%.

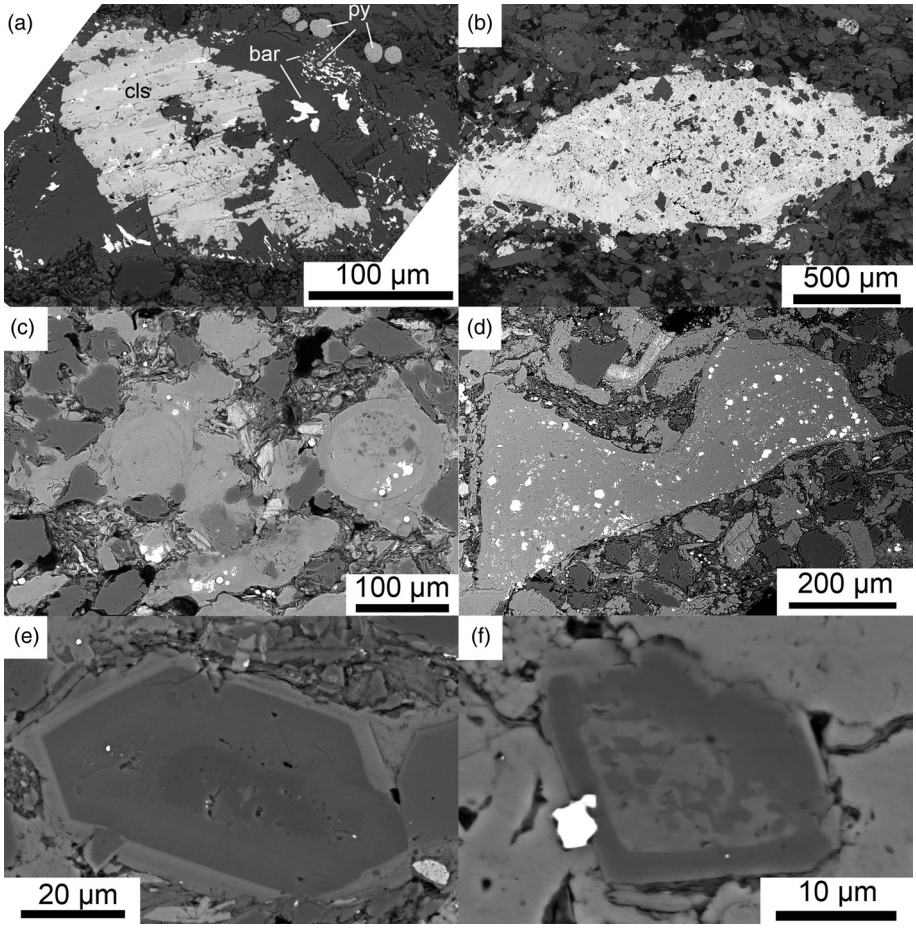

Fig. 7. Scanning electron microscopy backscattered electron images of Mochras sedimentary rock. (**a**) Aggregate of celestine and calcite with minor barite and pyrite framboids in sample SSK 74581 (991.49 m depth; Pliensbachian, *margaritatus* Zone). (**b**) Lens of celestine with minor intergrown barite and euhedral calcite with remnant kerogen at its centre in sample SSK 34671 (1060.35 m depth; Pliensbachian, *ibex* Zone). (**c**) Bioclasts cemented with calcite in sample SSK 34693 (1041.81 m depth; Pliensbachian, *ibex* Zone). Minor dolomite and abundant pyrite framboids are usually present in association with shell fragments and macrofossil wood. (**d**) Overprinted shell fragment showing abundant pyrite, partially tracing growth increments in sample SSK 45682 (901.93 m depth; Pliensbachian, *margaritatus* Zone). (**e**) Typical dolomite grain showing an Mg-rich core and more Ca- and/or Fe-rich overgrowth in sample SSK 44999 (1037.74 m depth; Pliensbachian, *ibex* Zone). (**f**) Dolomite grain with complex inner structure, but typical rim of higher average atomic mass in sample SSK 44327 (934.82 m depth; Pliensbachian, *margaritatus Zone*).

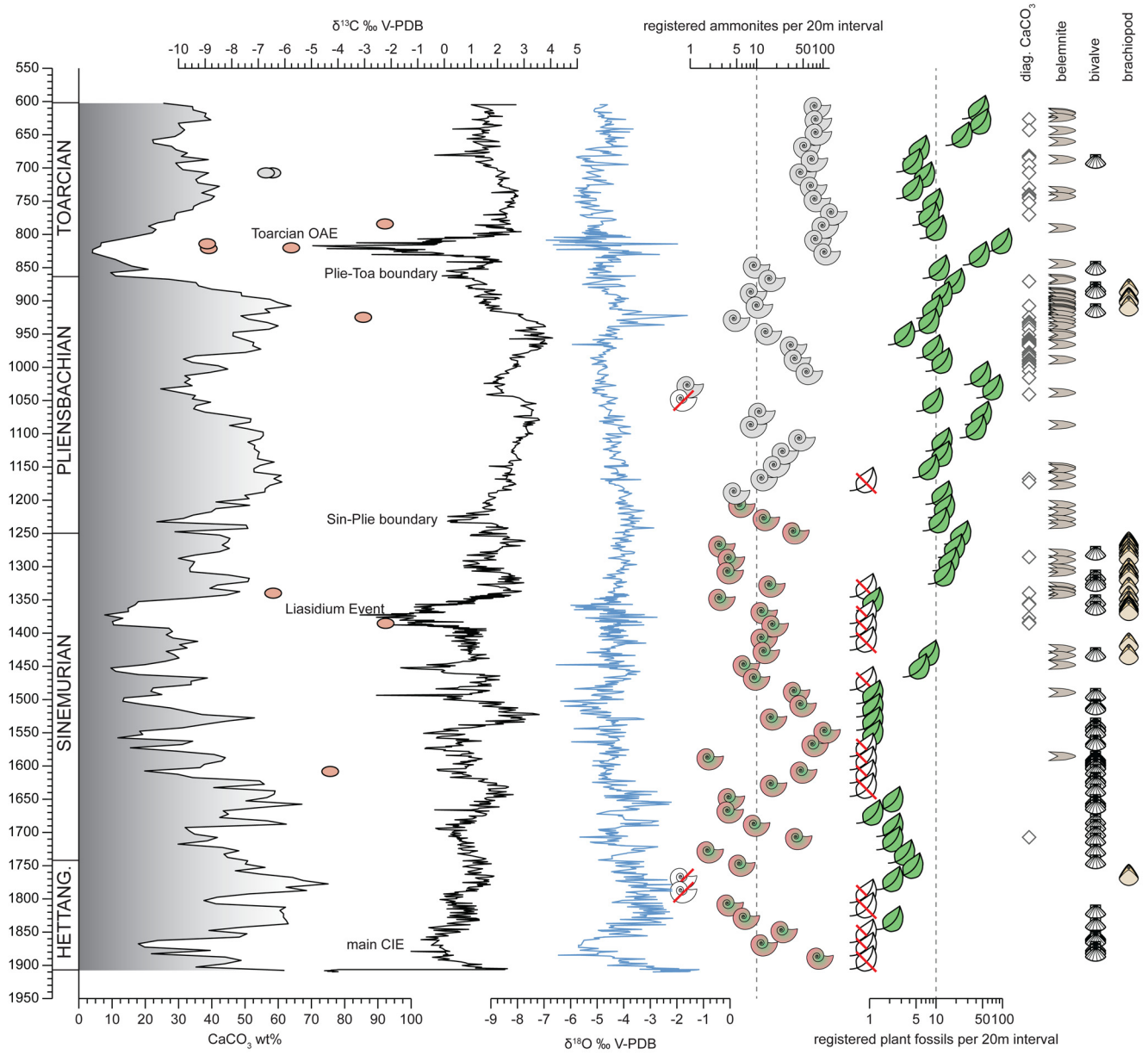

Fig. 8. Carbonate content, bulk carbonate $\delta^{13}C$ and $\delta^{18}O$ data, abundance of ammonite and fossil plant specimens per 20 m interval recorded in the registered specimen collection, and placement of macrofossils and diagenetic calcite samples measured in this study. The density of the plotted symbols for the various macrofossil groups gives a qualitative measure of the abundance of sufficiently large and well-preserved material for geochemical analysis.

The O isotope ratios in bulk carbonate show a much lower variability than the bulk C isotope ratios, with 95% of the data (n = 1188) falling into the range −5.7 to −2.5‰ V-PDB (median −4.4‰ V-PDB) and a total range from −8.7 to −0.8‰ V-PDB, and they do not correlate strongly with $\delta^{13}C_{carb}$ ($r^2 = 0.03$, $n = 1188$). However, the $\delta^{18}O$ values show a considerably higher high-frequency variability than the C isotope ratios and gentle (sub-per-mil) shifts over several hundred metres, but clear stratigraphic patterns are not indicated.

Bulk rock samples and nodules with red coloration indicative of the presence of siderite or other Fe-rich carbonate phases show C isotope ratios that are consistently more negative than the adjacent bulk rock samples and O isotope ratios that are less negative (Fig. 8).

Vein carbonate

The C and O isotope ratios of diagenetic calcite, such as slickenside mineralization and veins, show ranges comparable with those observed for bulk rock samples (Fig. 10). The $\delta^{13}C_{carb}$ values in vein calcite ($n = 243$) range from −1.8 to +4.2‰ (average +2.2‰) and $\delta^{18}O_{carb}$ from −9.0 to 0.0‰ (average −6.0‰). Samples of pure calcite from the Pliensbachian *jamesoni* Zone and deeper in the core show a strong, linear negative correlation of $\delta^{18}O$ with depth, with a slope of *c.* −5‰ km^{-1}. The robustness of this observation, however, is questionable as it is based on data from only seven specimens as a result of the limited number of calcite occurrences in this depth interval. Carbonate from two specimens of nodular siderite from the Sinemurian *obtusum* Zone shows much lower and variable $\delta^{13}C_{carb}$ ($n = 3$) ranging from −12.5 to −4.9‰ and $\delta^{18}O$ from −1.1 to +1.1‰.

The C and O isotope ratios of diagenetic phases are generally similar or related to those of the adjacent bulk rock, with median offsets of −0.3‰ for $\delta^{13}C_{carb}$ and −1.0‰ for $\delta^{18}O_{carb}$ (Fig. 10). Toarcian samples ($n = 44$) tend to be similar to the adjacent bulk rock, with median offsets of +0.2‰ for $\delta^{13}C_{carb}$ and +0.1‰ for $\delta^{18}O_{carb}$. The Pliensbachian samples ($n = 166$) are depleted, with median offsets of −0.5‰ for $\delta^{13}C_{carb}$ and −1.1‰ for $\delta^{18}O$. The Sinemurian ($n = 23$) samples are less depleted in C isotope ratios,

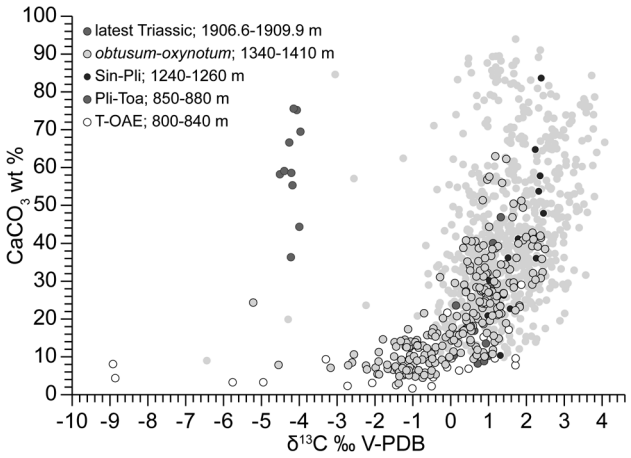

Fig. 9. Co-variation of calcite content with C isotope ratios in the Mochras core. Samples with $\delta^{13}C$ values less than −1‰ are almost exclusively observed in the carbonate-lean intervals of the Toarcian oceanic anoxic event and the *obtusum* and *oxynotum* Zones.

with median offsets of −0.1‰ for $\delta^{13}C_{carb}$, but more depleted in $\delta^{18}O_{carb}$ (median offset −3.1‰), extending a general trend to more ^{18}O depleted diagenetic calcite downcore.

Macrofossil calcite

The general rarity of well-preserved macrofossils in strata deposited during known intervals of major environmental perturbations precludes the geochemical assessment of how these events were recorded in biota in the Cardigan Bay Basin. Long-term trends of C and O isotope signatures can, however, be appraised.

The macrofossil calcite record is dominated by bivalves for the Hettangian and lower Sinemurian part of the core and by belemnites for the upper Sinemurian and above. The data show systematic trends in C isotope ratios throughout the entire length of the core (Fig. 11). $\delta^{13}C_{carb}$ values of *c.* +1.5‰ are recorded in the Hettangian and start to rise in the Sinemurian, reaching *c.* +3‰ in the *turneri* Zone. Here, a trend towards more negative values starts that culminates around the Sinemurian–Pliensbachian boundary, with $\delta^{13}C_{carb}$ values of *c.* −0.5‰. Stratigraphically above this minimum, values gradually rise to reach maximum values of *c.* +3‰ again in the uppermost Pliensbachian *spinatum* Zone. The $\delta^{13}C_{carb}$ values then show another broadly decreasing trend, reaching values near 0‰ in the uppermost Toarcian.

O isotope ratios of *c.*−2.5‰ are recorded in the Hettangian, with a general increase to *c.* −1.5‰ in the Sinemurian *bucklandi* Zone. $\delta^{18}O_{carb}$ then returns to more negative values of *c.* −2.5‰ in the *turneri* Zone, where a general increase in $\delta^{18}O_{carb}$ values is sustained to the Pliensbachian *jamesoni* Zone, with values of *c.* −0.5‰. Here, the O isotope ratios begin to decrease upwards once more, but a lack of fossil coverage precludes an assessment of the trend up to the *margaritatus* Zone, where $\delta^{18}O_{carb}$ reaches maximum values of more than +1‰. From this maximum, the values generally decrease upwards to the top of the Toarcian, with belemnites typically recording $\delta^{18}O_{carb}$ values of −2 to −1‰ above the T-OAE interval.

Carbonate element/Ca ratios

Vein calcite

All the analysed vein and slickenside carbonate can be classified as low-Mg-calcite with Mg/Ca ratios ranging from 2.5 to 27.0 mmol mol^{-1} (Supplementary data). The highest Mg/Ca ratios are found in slickensides and thin veins, whereas the widest veins and veins with the largest grain size tend to have low Mg/Ca ratios. The Sr/Ca ratios are highly variable, ranging from 0.41 to 137 mmol mol^{-1}, but all the samples with Sr/Ca ratios >5.5 mmol mol^{-1} show very similar S/Ca ratios (Fig. 12). No such co-variation is observed for samples with lower Sr/Ca ratios, however. A bimodal distribution is seen among the samples with Sr/Ca ratios <5.5 mmol mol^{-1}. A larger population comprising about two-thirds of the samples has a mode of *c.* 1 mmol mol^{-1} and the remaining third a mode of *c.* 3.5 mmol mol^{-1} (Fig. 12).

The Mn/Ca ratios are generally low, ranging from 0.24 to 7.5 mmol mol^{-1} (median 0.4 mmol mol^{-1} and 198 of 225 measurements <1 mmol mol^{-1}). All samples with Mn/Ca ratios >3 mmol mol^{-1} come from Sinemurian strata, with the enclosing bulk rock having mostly <20 wt.% carbonate content, whereas the Mn/Ca ratios in the samples from generally carbonate-rich Pliensbachian

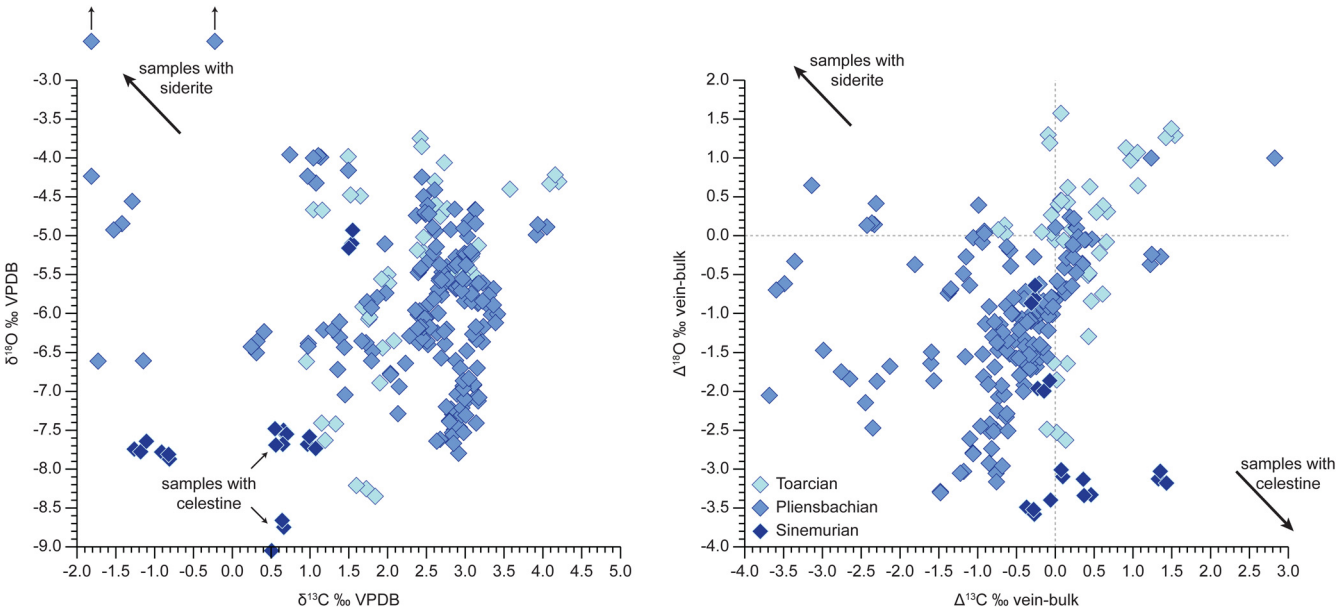

Fig. 10. C and O isotope data for diagenetic calcite. Left-hand panel: measured $\delta^{13}C$ and $\delta^{18}O$ values; right-hand panel: isotopic differences between diagenetic calcite and the adjacent bulk rock material.

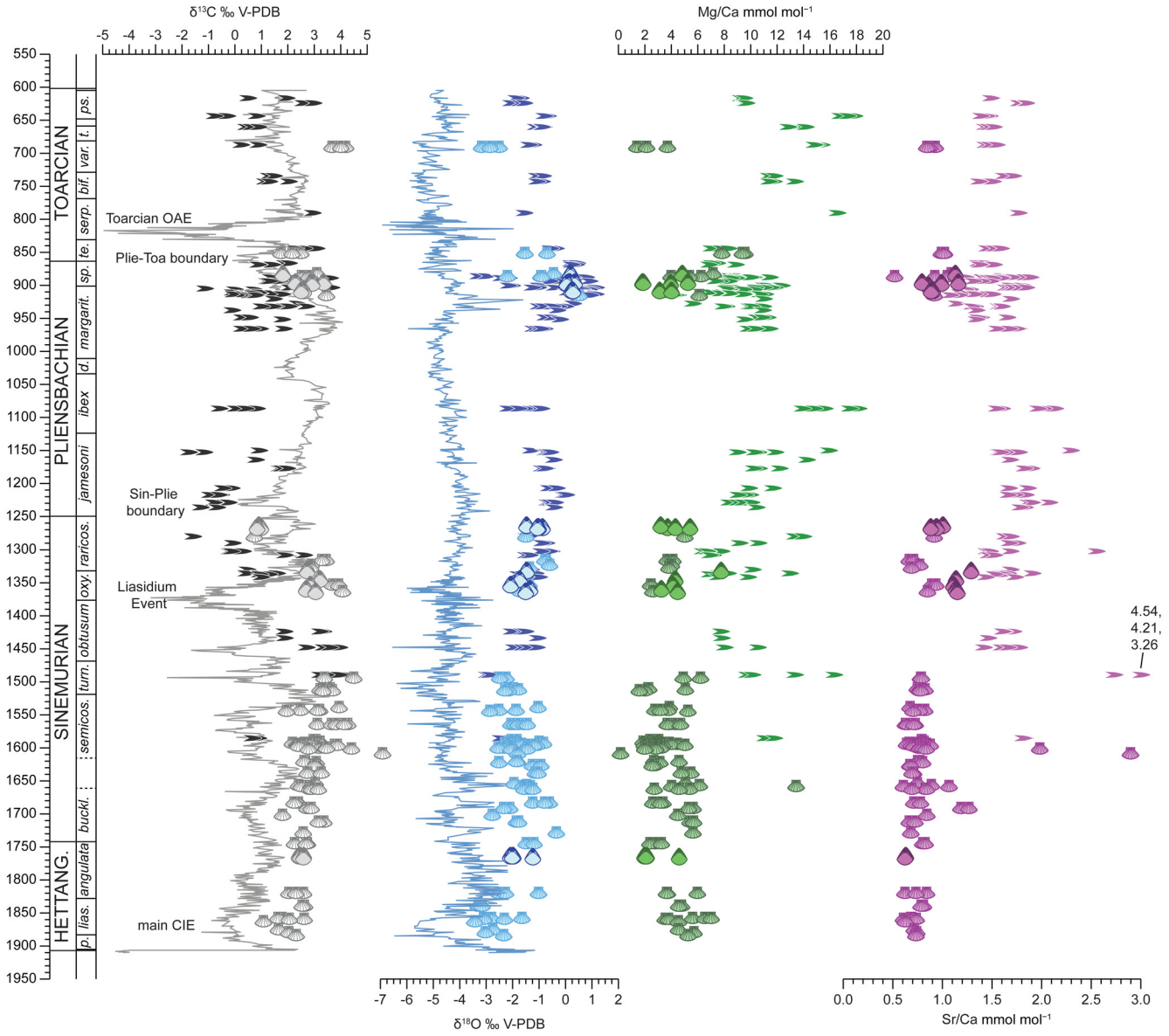

Fig. 11. Macrofossil C and O isotope ratios and Mg/Ca and Sr/Ca ratios.

rocks are consistently <0.8 mmol mol^{-1}. Qualitatively, the same trends also hold for the Fe/Ca ratios, but the latter are much more variable, ranging from 0.0 to 37.5 mmol mol^{-1} (median 0.4 mmol mol^{-1}) and show much larger stratigraphic variability.

Macrofossil calcite

The majority of bivalve data from the Hettangian and Sinemurian part of the core are from oysters, for which the Sr/Ca ratios consistently fall in the range 0.6–0.9 mmol mol^{-1}, without any clear stratigraphic trend. For the same samples, a slight decrease is indicated in the Mg/Ca ratio from the Hettangian (4.6 ± 0.6 mmol mol^{-1}, $n = 18$) to the Sinemurian (3.7 ± 0.4 mmol mol^{-1}, $n = 69$). Bivalve samples from the upper part of the core (the Pliensbachian *margaritatus* Zone to the Toarcian *variabilis* Zone) are chemically more variable, with Sr/Ca ratios typically *c.* 1 mmol mol^{-1} and Mg/Ca ratios from 1.4 to 9.6 mmol mol^{-1}.

Brachiopod samples from the Hettangian and upper Pliensbachian part of the core show Sr/Ca and Mg/Ca ratios coincident with those of the bivalve samples, whereas brachiopod material from the upper Sinemurian is enriched in both Sr/Ca (1.11–1.29 mmol mol^{-1}) and Mg/Ca (3.2–7.8 mmol mol^{-1}) compared with bivalves from the same interval.

Belemnite calcite consistently shows the highest Sr/Ca and Mg/Ca ratios of the three studied fossil groups, with Sr/Ca generally falling into the range 1.3–2.3 mmol mol^{-1}. One specimen from the Sinemurian *turneri* Zone and a single sample from the *raricostatum* Zone, however, show highly elevated Sr/Ca ratios of 2.6–4.5 mmol mol^{-1}. The Mg/Ca ratios in belemnite rostra range from 4 to 18 mmol mol^{-1}, with the lowest Mg/Ca ratios observed in the upper Sinemurian and upper Pliensbachian strata.

Discussion

Diagenetic history of the Mochras core

Diagenetic changes to the material in the Mochras core can be traced by visual core inspection, petrographic work and evidence from geochemical analyses of different carbonate phases. Lithification of the core was only rarely associated with the formation of clearly nodular levels, at least in the Pliensbachian and Toarcian, for which the archive core is still preserved and the core is of sufficient

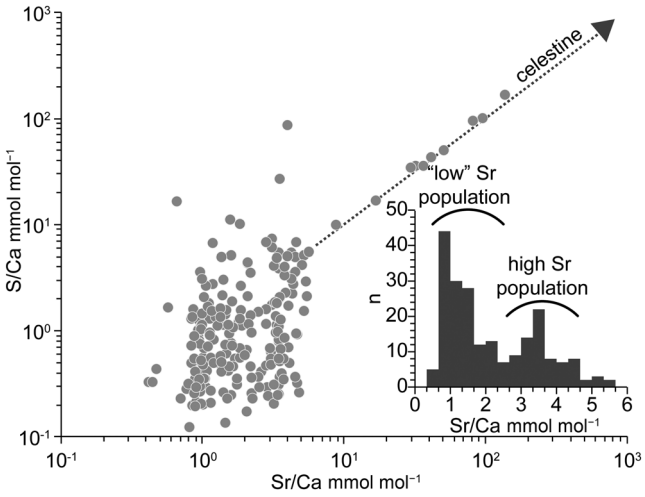

Fig. 12. Sr/Ca ratios v. S/Ca ratios in diagenetic carbonate samples showing elevated Sr and the clear co-variation of S with Sr at very high Sr, suggestive of the contribution of celestine to the bulk signature. Inset shows histogram of Sr/Ca ratios in samples for which no clear celestine component is apparent from the S/Ca data.

diameter to allow the identification of nodules up to *c.* 20 cm in size. Carbonate cementation and sharp contrasts in sediment colour, however, are commonly observed, suggesting that nodule formation might more often have progressed to form continuous limestone bands or nodules much larger than the diameter of the core.

Abundant siderite has been observed in the *tenuicostatum* and *serpentinum* Zones of the Toarcian as brown–red coloured nodules and bands in the archive core, via X-ray diffraction analysis and through a strongly enhanced Fe signal in the p-XRF measurements (Xu *et al.* 2018*a*). The formation of the Toarcian siderite nodules has previously been linked to early diagenetic growth in an environment with a low availability of sulfate, but high levels of Fe^{2+} and carbonate ions (Curtis and Spears 1968; Xu *et al.* 2018*a*). Septarian siderite nodules have also been found in the aggregate reserve bags in the Sinemurian *obtusum* Zone at depths of 1385–1387 m.

Isotopic analysis ($n = 3$, Supplementary table 7) of these materials yielded $\delta^{13}C_{carb}$ values of −12.5 to −4.9‰, substantially lower than adjacent bulk rock samples, which averaged −1.0‰ ($n = 34$) in the stratigraphic interval from 1380 to 1390 m depth. The $\delta^{18}O_{carb}$ values of −1.1 to +1.1‰, on the other hand, are less negative than the nearby bulk calcite, which averages −4.0‰ in the same interval, in places even yielding $\delta^{18}O_{carb}$ values >0‰. One of the two *obtusum* Zone nodules (SSK 78968) formed around an ammonite, the shell of which is still preserved as iridescent aragonite, and showed septarian cracks filled with celestine (Fig. 5).

Published equilibrium O isotope fractionation factors for siderite vary greatly (e.g. Mortimer and Coleman 1997; Hałas and Chlebowski 2004), complicating estimates of the formation temperature and/or fluid $\delta^{18}O_{siderite}$ from these nodules. The $\delta^{18}O_{siderite}$ values from siderite can therefore not confidently be used at the present time to interpret the timing and mechanisms of formation (see also Huggett *et al.* 2000). Low $\delta^{13}C_{carb}$ values, however, suggest that C derived from the oxidation of organic matter and/or microbial processes was present during their formation, whereas residual C from methanogenesis probably had no significant role (Irwin *et al.* 1977; Pearson and Nelson 2005). The preferential occurrence of siderite nodules around the early Toarcian and Sinemurian *obtusum*/*oxynotum* Zones points to specific depositional and/or post-depositional conditions experienced in the Cardigan Bay Basin that were met during both these episodes of environmental perturbation.

Nodular levels in the Pliensbachian *margaritatus* Zone are calcitic rather than sideritic. Bedding and bioturbation are deformed around these nodules (Fig. 4b), providing evidence that they formed before the lithification and compaction of the sediment had been completed.

The C isotope ratios of bulk carbonate are mostly positive and the $\delta^{18}O$ values not highly negative, suggesting that neither meteoric diagenesis nor deep burial pervasively overprinted the geochemical signatures in the core (Lohmann 1983; Al-Aasm and Veizer 1986*a*; Ullmann and Korte 2015). The bulk O isotopic ratios, however, are too low and variable to be reflective of the environmental conditions and do not match the patterns recorded in macrofossil calcite (Fig. 11). The same is true for the $\delta^{13}C_{carb}$ values, which – despite their systematic stratigraphic trend – show clear offsets from the macrofossil calcite and partially negative values. This is particularly clear around intervals of known environmental perturbation such as the T-OAE (e.g. Hesselbo *et al.* 2000; Kemp *et al.* 2005; Suan *et al.* 2008; Hermoso *et al.* 2012; Ullmann *et al.* 2020) and the Sinemurian Liasidium event (Riding *et al.* 2013; Hesselbo *et al.* 2020*b*), where the carbonate content in the core is very low (Figs 3 and 8). It is therefore most probable that most of the bulk carbonate was formed before deep burial and partly under the influence of oxidized organic matter (Okita *et al.* 1988), which led to the $^{13}C_{carb}$ depletion, which is most pronounced where the carbonate content is low and the total organic carbon content is comparatively high.

The O isotope ratios of Hettangian samples of −6 to −2‰ in the Mochras bulk carbonate are broadly similar, but less negative than ratios in samples from the Somerset coast (−7 to 3‰, Clémence *et al.* 2010) and the Dorset coast (−6 to 4‰, Schöllhorn *et al.* 2020). All three sequences share a tendency of lower $\delta^{18}O$ in the lower Hettangian, which has been ascribed to freshening and/or warming (Schöllhorn *et al.* 2020). However, it is unclear to what degree this signal could be preserved in bulk rock sequences given the strong deviation from macrofossil values (Hesselbo *et al.* 2020*c*). The O isotope ratios in the Sinemurian and Pliensbachian of the Wessex Basin are more variable and initially more negative than at Mochras (Schöllhorn *et al.* 2020), suggesting lower temperatures and/or less influence of freshwater during diagenetic stabilization of the rock in the Cardigan Bay Basin. The $\delta^{13}C_{carb}$ values in the Wessex Basin are typically *c.* 2‰ lower than in the Cardigan Bay Basin in Hettangian and Sinemurian strata and are scattered where the carbonate content is <10%, even though a broad correspondence of isotopic excursions in organic matter and carbonate is observed (Schöllhorn *et al.* 2020). Deviations of $\delta^{13}C_{carb}$ from the original values may have been amplified in carbonate-lean intervals, but prominent excursions were not entirely erased by this process.

The formation of veins and slickensides at Mochras probably occurred over multiple phases, with the geochemical and petrographic evidence pointing to the earliest veins and cracks having been at least partially formed by celestine and subordinate barite. Later destabilization of sulfate minerals led to partial replacement with low-Mg-calcite, which shows distinct Sr enrichment where celestine precursors were present. Remnants of earlier celestine partially replaced by calcite were observed using geochemical and petrographic methods (Figs 6 and 12). Strong veining is restricted to the middle to upper Toarcian and the Pliensbachian *margaritatus* Zone, whereas veins in the lower Pliensbachian and upper Sinemurian are sporadic and virtually absent at depths >1400 m. Sediment shearing is also observed in the Hettangian and Sinemurian part of the core, but is manifested by striated surfaces with an oily shine rather than precipitates of calcite. The generally close correspondence of C isotope ratios and only slight depletion of ^{18}O in veins and slickensides with respect to the enclosing bulk rock (Fig. 10) suggests that much of the C in their calcite was locally sourced and formation did not take place during deep burial. Whether the concentration of particularly wide, coarse-

grained veins in the *margaritatus* Zone rocks has a structural origin (e.g. local extension as a consequence of activity on the Mochras fault; Holford *et al.* 2005) is not clear. A gap in veining in the very carbonate-lean T-OAE interval in the lower Toarcian suggests that the availability of carbonate in the formation may have impacted the viability and style of vein formation in the lithified strata. By contrast, the lack of veins in the carbonate-rich Hettangian suggests that the availability of carbonate was not the only driving factor.

Macrofossils underwent diagenesis under conditions that were seemingly similar to those during vein formation. Geochemical data from three samples of a single echinoid fragment (SSK 78721, 936 m, *margaritatus* Zone) should record early diagenetic stabilization and cementation of the original porosity (Al-Aasm and Veizer 1986*a*; Swart 2015). The samples show the addition of Mn and Fe as well as $\delta^{18}O$ values similar to nearby calcite veins. The composite skeletal and diagenetic calcite seemingly retained part of its original geochemical fingerprint (Dickson 2001; Gorzelak *et al.* 2016), however, showing high Mg/Ca ratios averaging 27 mmol mol^{-1} and a high $\delta^{13}C_{carb}$ value of +3.9‰. Even the most altered fossil material and cements filling fossil cavities are not as highly depleted in $^{13}C_{carb}$ or $^{18}O_{carb}$ as in some other UK sequences of similar age (Saelen *et al.* 1996; Hesselbo *et al.* 2020*c*; minimum observed values in Mochras are −1.4‰ for $\delta^{13}C_{carb}$ and −5.9‰ for $\delta^{18}O_{carb}$).

Diagenetic Fe enrichment in the fossil calcite is much stronger than Mn enrichment, with maximum Mn/Ca ratios of 1.7 mmol mol^{-1} and highest Fe/Ca ratios of 5.3 mmol mol^{-1} observed in belemnite calcite. The Mn/Ca ratios in the Toarcian alveolar cements, reaching up to 1.1 mmol mol^{-1}, are much lower than those of Toarcian cements in the Cleveland Basin (>4 mmol mol^{-1}, Ullmann *et al.* 2015), but slightly higher than those from the Toarcian of the Iberian Basin (*c.* 0.8 mmol mol^{-1}; Ullmann *et al.* 2020). No clear depletion of Sr during recrystallization is observed in the Mochras material, with neither belemnites ($n = 171$; $r^2 = <0.01$), bivalves ($n = 124$; $r^2 = 0.01$) nor brachiopods ($n = 35$; $r^2 = 0.25$) showing a strong, negative relationship with Mn (the weak co-variation for brachiopods has a positive slope). This observation is in contrast with the typically distinct negative co-variation of Mn with Sr, observed, for example, in the Sr-rich belemnite rostra elsewhere (e.g. Al-Aasm and Veizer 1986*b*; Ullmann *et al.* 2013, 2015; Ullmann and Korte 2015). Sr was therefore probably available in abundance in pore fluids, as is further evidenced by the observation of celestine veins that may have formed in response to Sr-enriched pore waters after the dissolution of Sr-rich biogenic carbonate (Hoareau *et al.* 2010). This lack of Sr depletion tentatively places the majority of the geochemical overprint on macrofossils into the interval when calcite vein formation and celestine breakdown occurred.

Bulk rock signals relating to environmental change

The Mochras bulk carbonate (and organic matter) record has yielded clear $\delta^{13}C_{carb}$ excursions that coincide with known phases of environmental and C cycle perturbation (Figs 8, 11 and 13), the most prominent being the T-OAE (Jenkyns *et al.* 2002; van de Schootbrugge *et al.* 2005*a*). Other Mochras isotope excursions that

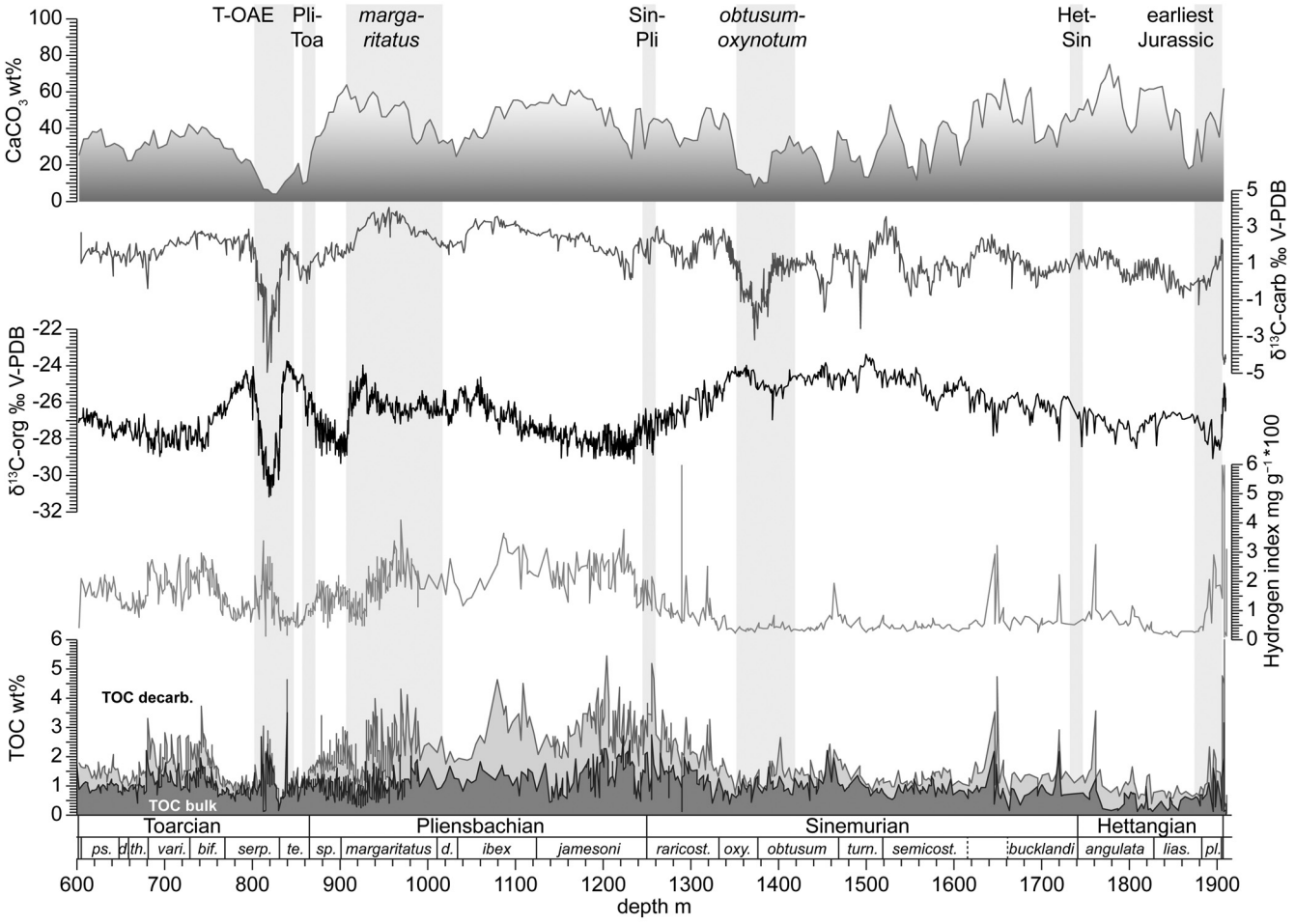

Fig. 13. Bulk rock carbonate content, carbonate and organic matter $\delta^{13}C$, hydrogen index and percentage total organic carbon (TOC) plotted as fraction of the whole rock (dark grey) and decarbonated residue (light grey). Carbonate data include compiled values from Jenkyns *et al.* (2002) and Katz *et al.* (2005) and the organic data are taken from Xu *et al.* (2018*a*) and Storm *et al.* (2020).

are equally visible in the Mochras $\delta^{13}C_{org}$ record (Xu *et al.* 2018*a*; Storm *et al.* 2020, Fig. 13) can be matched with the main isotope excursion following the end-Triassic mass extinction (e.g. Hesselbo *et al.* 2002; Ruhl *et al.* 2009, 2010), the *obtusum*/*oxynotum* Zones or the 'Liasidium event' (Riding *et al.* 2013; Hesselbo *et al.* 2020*b*), the Sinemurian–Pliensbachian boundary (Korte and Hesselbo 2011; Duarte *et al.* 2014; Peti *et al.* 2017), the *margaritatus* Zone positive excursion (Jenkyns and Clayton 1986; Korte and Hesselbo 2011; Mercuzot *et al.* 2020) and the Pliensbachian–Toarcian boundary (Hesselbo *et al.* 2007; Littler *et al.* 2010; Bodin *et al.* 2016).

Apart from the *margaritatus* Zone excursion or 'Late Pliensbachian event' *sensu* Korte and Hesselbo (2011), all these excursions are characterized by a transient decrease in carbonate content, suggesting that carbonate production was adversely affected locally. Although this transient loss of carbonate underlines that these environmental perturbations substantially impacted the Cardigan Bay Basin depositional environment, it also created geochemical conditions that make diagenetic overprints of the bulk carbonate signature more prominent. In addition to the T-OAE interval, this is particularly clear in the Sinemurian *obtusum* and *oxynotum* Zones, where the second largest Early Jurassic bulk carbonate C isotope perturbation in the Lower Jurassic of the Mochras core is recorded (Fig. 13). This event is smaller in amplitude, but otherwise shares a number of geochemical characteristics with the T-OAE, including the presence of siderite, amplified bulk carbonate C isotope excursion and the loss of carbonate and well-preserved remains of large fossils. A clear stratigraphic offset between a negative C isotope excursion observed in bulk organic matter (Storm *et al.* 2020) and in carbonate in this interval illustrates this complex interplay of environmental change and diagenesis.

Although the diagenetic enhancement of bulk carbonate C isotope excursions is fortuitous for broad stratigraphic correlation, it signifies the vulnerability of bulk carbonate in Mesozoic environments to post-depositional alteration (cf. Weissert *et al.* 1979; Ruebsam and Al-Husseini 2020). Diagenetically induced shifts in carbonate $\delta^{13}C$ values that show stratigraphic changes in magnitude also complicate considerations of C cycle dynamics, including the offset between carbonate and organic matter isotope records as a proxy for pCO_2 (van de Schootbrugge *et al.* 2005*a*). Bulk carbonate chemostratigraphic records have to be interpreted very cautiously, even where correlatable isotope perturbations are observed, because their amplitude, exact stratigraphic extent and absolute values are likely to be biased as a consequence of diagenetic overprints. Furthermore, additional isotope excursions may be induced by locally variable diagenetic conditions that could be misread as reflecting true environmental perturbations. Isotope shifts, for example, occur in the lower *obtusum* Zone at *c.* 1450 m depth and the *jamesoni* Zone at *c.* 1190 m depth, and both coincide with increases in total organic carbon and the hydrogen index as well as a loss of carbonate (Fig. 13). Although such excursions might be the manifestation of local or even regional events, they could also be preservational artefacts.

Macrofossil record

The macrofossil record of the Mochras core reflects biotic changes, environmental trends and perturbations that are already well established in other UK sedimentary archives and across the globe (Fig. 14). As in other UK sections, the macrofossil material from the Hettangian to Sinemurian, the size and preservation of which makes it relevant for geochemical analysis, is dominated by bivalves (Jones *et al.* 1994; Korte *et al.* 2009; Hesselbo *et al.* 2020*b*). As is common in UK successions, the macrofossils of sufficient size and quality for analysis in Pliensbachian and Toarcian strata are primarily belemnite rostra, supplemented by bivalves and brachiopods (Jones *et al.* 1994; McArthur *et al.* 2000; Korte and Hesselbo 2011; Korte *et al.* 2015). The phases of pronounced environmental change are often characterized by a reduction in the abundance of macrofossils, as, for example, seen previously for belemnites during the T-OAE (Hesselbo *et al.* 2007; Rita *et al.* 2019; Ullmann *et al.* 2020). This effect is magnified in core material such as the Mochras core (Xu *et al.* 2018*a*), where the scarcity cannot be counteracted by more comprehensive lateral sampling coverage of the outcropping strata. The episodic reductions in fossil abundance are probably a reflection of transiently deteriorating conditions for macrofaunal life, both benthic and nektonic, in the Cardigan Bay Basin. However, in the core intervals where macrofossil material of sufficient quality is absent, it is not possible to carry out quantitative geochemical assessments of local environmental change, including intervals such as the earliest Jurassic, Sinemurian *obtusum*/*oxynotum* Zones and the T-OAE. Longer term shifts in climate conditions are, however, clearly imaged (Fig. 14).

Isotopic trends in the UK Early Jurassic

A generally increasing trend of $\delta^{13}C$ in macrofossil calcite and organic matter from the mid-Hettangian, reaching an optimum around the Sinemurian *turneri* Zone, matches a recent compilation of data from the Bristol Channel and Hebrides basins (Figs 11, 13 and 14; Hesselbo *et al.* 2020*c*) and Europe in general (Dera *et al.* 2011). The isotope record of the Cleveland Basin is the best established for the upper Sinemurian to upper Toarcian of the UK (Bailey *et al.* 2003; Korte and Hesselbo 2011; Korte *et al.* 2015). The Mochras macrofauna matches the general trends very well, but from the Sinemurian *raricostatum* Zone onwards mostly follows the lower end of the $\delta^{13}C$ range and the higher end of the $\delta^{18}O$ range recorded in the Cleveland Basin. Broad $\delta^{18}O$ maxima are found in the Sinemurian *bucklandi* Zone and the Pliensbachian *jamesoni* and *margaritatus* Zones.

These maxima match observations from other UK basins (Korte and Hesselbo 2011; Korte *et al.* 2015; Hesselbo *et al.* 2020*c*) and all post-date spikes in the abundance of macrofossil wood in the core. The intervals in the Mochras core that show relative enrichments in macrofossil wood – notably the *angulata*, *obtusum*, upper *raricostatum*, *davoei*, *serpentinum* and *levesquei* Zones – instead coincide with comparatively negative macrofossil $\delta^{18}O$ values in other UK basins (Korte and Hesselbo 2011; Korte *et al.* 2015; Hesselbo *et al.* 2020*c*) and the rarity or absence of well-preserved shell material in the core record (Fig. 14). This is particularly prominent in the Pliensbachian *davoei* Zone and during the T-OAE interval, peaking in the *serpentinum* Zone of the Toarcian (Fig. 14).

Apart from the wood peak of the T-OAE, which is accompanied by mass transport deposits (Xu *et al.* 2018*a*), all other enrichments in macrofossil wood coincide with intervals recognized as phases of low relative sea-level in the UK region (Hesselbo 2008). It is therefore possible that the abundance of wood may correspond to the proximity of terrestrial flora to the site of deposition, the area of land masses in the epicontinental seaway hosting terrestrial macroflora, or the extent of their river catchment areas. Broad trends in the O isotope records of benthic and nekto-benthic organisms through the Early Jurassic may then be read as changes in bottom water temperatures due to changing water depths (Korte and Hesselbo 2011), perhaps amplified by the admixture of a freshwater component, as previously hypothesized for major climate change intervals (Saelen *et al.* 1996; van de Schootbrugge *et al.* 2005*b*; McArthur *et al.* 2008; Dera and Donnadieu 2012).

However, it is not excluded that the spikes in wood abundance could also have been the consequence of warmer climates, promoting the denser growth of large, terrestrial vegetation. A broad pattern of increasing kaolinite abundance from the *jamesoni*

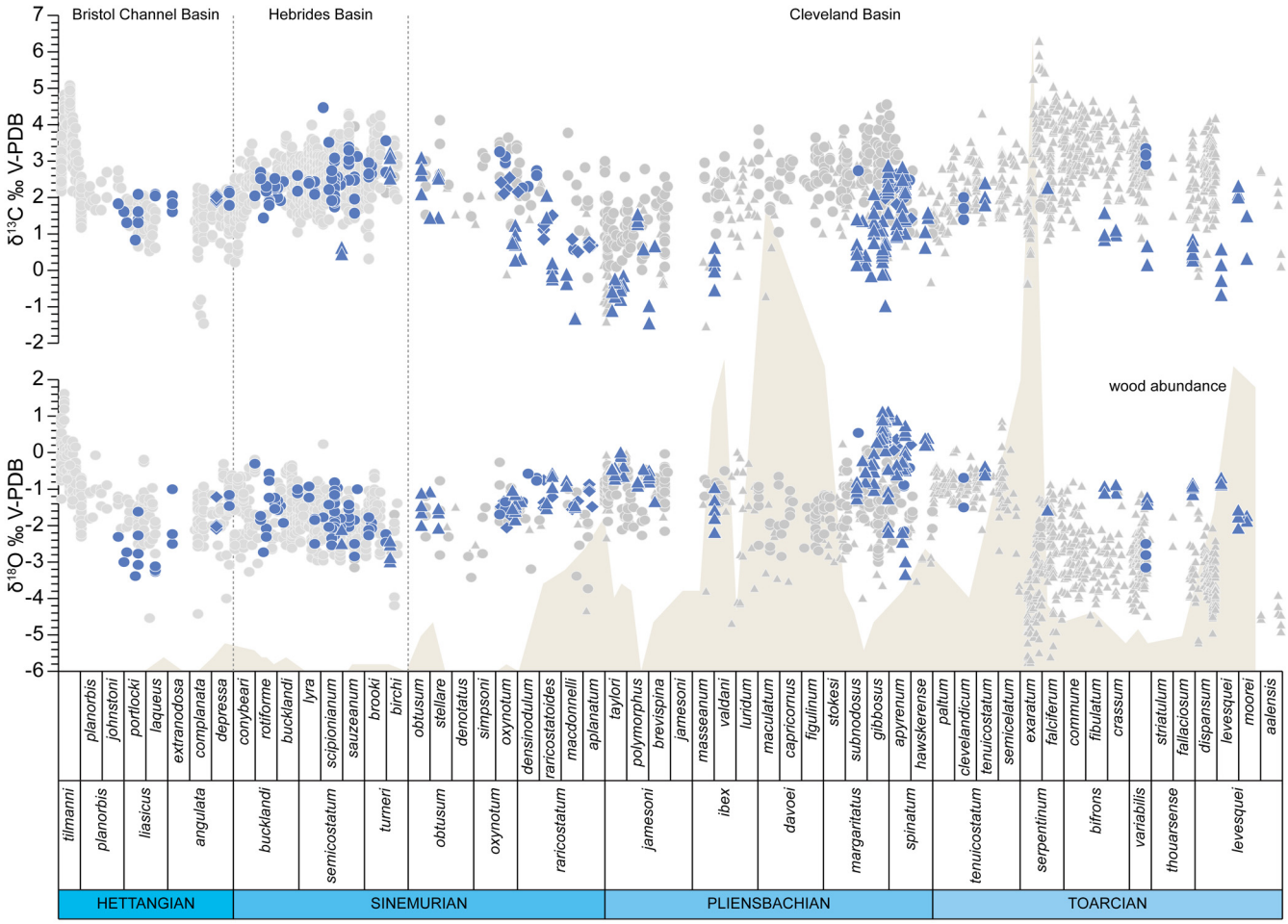

Fig. 14. Mochras macrofossil C and O isotope record (blue symbols) compared with published data from other UK basins taken from Korte and Hesselbo, (2011), Korte *et al.* (2015) and Hesselbo *et al.* (2020*c*). The light grey shaded area represents the relative abundance of macrofossil wood in the Mochras core based on the number of registered macrofossil wood and fossil plant specimens per 20 m of core interval as presented in Figure 7. The circles denote bivalve samples, the diamonds represent brachiopod samples and the triangles represent belemnite samples.

to *davoei* Zones and from the *tenuicostatum* to *bifrons* Zones has been observed in a number of European basins (Dera *et al.* 2009; Fantasia *et al.* 2018, 2019). An increase in kaolinite has also been seen towards the end of the Pliensbachian in northern Spain (the Asturian Basin; Deconinck *et al.* 2020). Currently available clay mineral data for the upper Sinemurian to top Pliensbachian of the Mochras core (Deconinck *et al.* 2019; Munier *et al.* 2020) show a series of increased kaolinite/illite ratios. These phases are interpreted as indicative of humid climates and occur in the lower *obtusum*, lower *oxynotum* and *raricostatum* Zones in the Sinemurian, and the *jamesoni*, *davoei* and *spinatum* Zones in the Pliensbachian. Within the constraints of sample resolution, these increases in the importance of kaolinite coincide with greater numbers of registered macrofossil wood specimens, supporting the hypothesis of a climatic control on the abundance of macrofossil wood in the Mochras core. By extension, broader minima in macrofossil $\delta^{18}O$ connected with warming effects, possibly also associated with an increased meteoric component of local seawater, is qualitatively supported by these data. The magnitude of wood peaks, however, varies strongly, increasing towards the Pliensbachian *davoei* Zone, suggesting an additional role of the local palaeogeography and depositional setting on changes in absolute abundance through time.

Interbasinal differences in isotope trends

The reason for the lower isotopic variability in the Cardigan Bay Basin compared with the Cleveland Basin may be related to the palaeoceanographic conditions in the Laurasian epicontinental seaway. Although located only a few hundred kilometres to the west of the Cleveland Basin, the Cardigan Bay Basin belemnite C and O isotope signatures are similar to all other belemnite records of European basins for which the data coverage is reasonable at least for parts of the upper Sinemurian–Toarcian. The O and C isotope ratios in the uppermost Sinemurian–Toarcian belemnites from the Mochras core are similar to those observed in Spain (the Basque-Cantabrian Basin, Rosales *et al.* 2004; the Asturian Basin, Gómez *et al.* 2008) and Ukraine/Slovakia (the Pienini Klippen Basin, Arabas *et al.* 2017). Upper Sinemurian–middle Pliensbachian belemnite data from the Wessex Basin (Price *et al.* 2016) and Pliensbachian–lower Toarcian belemnites from the Lusitanian Basin (Jenkyns *et al.* 2002) also show this similarity. Equally, upper Pliensbachian and lower Toarcian belemnite rostra from SW Germany (Bailey *et al.* 2003) and the French Grands Causses Basin (van de Schootbrugge *et al.* 2010) conform to the higher end of the $\delta^{18}O$ range and the lower part of the $\delta^{13}C$ range seen in the Cleveland Basin. Limited data from Scotland suggest a similar spread of isotope ratios in the Hebrides and Cleveland basins (Korte *et al.* 2015). The comparability of the Cardigan Bay data with more southerly basins makes it likely that the basin experienced conditions comparable with others nearer the open Tethys Ocean and argues for special environmental conditions within the Cleveland and more northerly basins. Os isotope data from the Toarcian at Mochras support a similar conclusion (Cohen *et al.* 2004; Percival *et al.* 2016).

A negative co-variation of $\delta^{13}C$ with $\delta^{18}O$ values was observed for belemnite rostra from the *falciferum* and *commune* subzones (upper *serpentinum* and lower *bifrons* Zones) in the Cleveland Basin (Ullmann *et al.* 2014). This co-variation was interpreted to reflect a vertical heterogeneity of temperature and the isotopic composition of dissolved inorganic carbon in local water masses, with the belemnites experiencing and recording different depths of the water column depending on the ecology and availability of oxygen. For example, shallow-dwelling belemnites would have sampled more productive and warmer surface waters than their deeper dwelling counterparts (Ullmann *et al.* 2014). The Cardigan Bay Basin belemnites, similar to their counterparts in basins closer to the Tethys Ocean, may thus predominantly record the bottom water conditions. Alternatively, the Cardigan Bay Basin (and other) belemnites may have been able to migrate into the Cleveland and more northerly basins at least episodically, where this signal was then preserved alongside local belemnites that had their own distinct geochemical signature.

The Sinemurian–Toarcian brachiopod record from the Lusitanian Basin (Ferreira *et al.* 2019) does not closely conform to the belemnite records of Cardigan Bay and other European basins, showing, on average, more negative $\delta^{18}O$ and more positive $\delta^{13}C$ values. This highlights that the immediate comparability of belemnite records with other macrofaunal datasets may be complicated by effects relating to the belemnite mode of life and possibly biomineralization (see also Voigt *et al.* 2003; Alberti *et al.* 2012 for geologically more recent examples). This discrepancy, however, does not impact on the observation that a geographical divide appears to exist among the belemnite datasets, which separates the Cleveland and Hebrides basins from the Cardigan Bay and more southerly basins. Whether the larger isotopic spread in the Cleveland Basin relates to local effects or the regional heterogeneity of water masses in the Laurasian Seaway cannot be confidently determined at the present time. Further research on macrofossil geochemistry from adjacent basins and added palaeogeographical constraints as derived, for example, from sediment provenance studies will help to identify broader patterns and the feasibility of migration routes for mobile marine animals.

Conclusions

The Mochras core yielded >1300 m of Early Jurassic mudstone without apparent large sedimentation breaks and constitutes a valuable resource for building a high-resolution, integrated stratigraphy for the Early Jurassic. Lithification and diagenetic modification of the sediment did not induce strong depletions in Sr, ^{13}C or ^{18}O in the carbonate phases, with diagenetic stabilization occurring before deep burial. However, the magnitude of C isotope excursions in bulk carbonate was amplified by a reduction in the carbonate content during environmental perturbations, increasing the biasing effect of added diagenetic carbonate containing C sourced from oxidized organic matter.

The macrofossil assemblages and geochemistry reinforce the long-term trends observed elsewhere in European Early Jurassic sequences. The rarity of macrofauna during large environmental perturbations illustrates the negative effects of such events on faunal assemblages.

The Mochras belemnite C and O isotope record follows the same trend as the well-established record of the nearby Cleveland Basin, but shows lower isotopic variability and a shift to comparatively low $\delta^{13}C$ and high $\delta^{18}O$ values. This shift may have been caused by distinct palaeoceanographic differences between these UK basins, such as connection to the open Tethys Ocean and susceptibility to influences from adjacent drainage basins.

Acknowledgements The reviews of an anonymous reviewer, Karem Azmy and Helmut Weissert helped us to improve the quality and clarity of this study. The authors thank the staff of the core store of the British Geological Survey at Keyworth for their help with sampling and curation of core materials. We thank Chris Mitchell (University of Exeter) for assistance with the isotopic analysis of bulk carbonate samples.

Author contributions **CVU:** conceptualization (lead), data curation (lead), formal analysis (lead), funding acquisition (supporting), investigation (lead), methodology (lead), project administration (lead), writing – original draft (lead), writing – review and editing (lead); **DS:** data curation (supporting), formal analysis (supporting), investigation (supporting), methodology (supporting), writing – review and editing (supporting); **MJ**: formal analysis (supporting), investigation (supporting), methodology (supporting), writing – review and editing (supporting); **AJLH**: formal analysis (supporting), investigation (supporting), methodology (supporting), writing – review and editing (supporting); **SPH**: conceptualization (supporting), formal analysis (supporting), funding acquisition (lead), investigation (supporting), methodology (supporting), project administration (supporting), writing – original draft (supporting), writing – review and editing (supporting).

Funding information This work was funded by the Natural Environment Research Council (NE/N018508/1).

Data availability All data generated during this study are included in the Supplementary information files for this article.

Scientific editing by Ashleigh Hood

References

Al-Aasm, I.S. and Veizer, J. 1986*a*. Diagenetic stabilization of aragonite and low-Mg calcite, II. Stable isotopes in rudists. *Journal of Sedimentary Petrology*, **56**, 763–770, https://doi.org/10.1306/212F88A5-2B24-11D7-8648000102C1865D

Al-Aasm, I.S. and Veizer, J. 1986*b*. Diagenetic stabilization of aragonite and low-Mg calcite, I. Trace elements in rudists. *Journal of Sedimentary Petrology*, **56**, 138–152, https://doi.org/10.2110/jsr.56.763

Alberti, M., Fürsich, F.T. and Pandey, D.K. 2012. The Oxfordian stable isotope record ($\delta^{18}O$, $\delta^{13}C$) of belemnites, brachiopods, and oysters from the Kachchh Basin (western India) and its potential for palaeoecologic, palaeoclimatic, and palaeogeographic reconstructions. *Palaeogeography, Palaeoclimatology, Palaeoecology*, **344–345**, 49–68, https://doi.org/10.1016/j.palaeo.2012.05.018

Arabas, A., Schlögl, J. and Meister, C. 2017. Early Jurassic carbon and oxygen isotope records and seawater temperature variations: insights from marine carbonate and belemnite rostra (Pieniny Klippen Belt, Carpathians). *Palaeogeography, Palaeoclimatology, Palaeoecology*, **485**, 119–135, https://doi.org/10.1016/j.palaeo.2017.06.007

Bailey, T.R., Rosenthal, Y., McArthur, J.M., van de Schootbrugge, B. and Thirlwall, M.F. 2003. Paleoceanographic changes of the Late Pliensbachian–Early Toarcian interval: a possible link to the genesis of an oceanic anoxic event. *Earth and Planetary Science Letters*, **212**, 307–320, https://doi.org/10.1016/S0012-821X(03)00278-4

Barron, A.J.M., Lott, G.K. and Riding, J.B. 2012. *Stratigraphical Framework for the Middle Jurassic Strata of Great Britain and the Adjoining Continental Shelf*. British Geological Survey.

Bodin, S., Krencker, F.-N., Kothe, T., Hoffmann, R., Mattioli, E., Heimhofer, U. and Kabiri, L. 2016. Perturbation of the carbon cycle during the late Pliensbachian–early Toarcian: new insight from high-resolution carbon isotope records in Morocco. *Journal of African Earth Sciences*, **116**, 89–104, https://doi.org/10.1016/j.jafrearsci.2015.12.018

Clémence, M.-E., Bartolini, A., Gardin, S., Paris, G., Beaumont, V. and Page, K.N. 2010. Early Hettangian benthic–planktonic coupling at Doniford (SW England): palaeoenvironmental implications for the aftermath of the end-Triassic crisis. *Palaeogeography, Palaeoclimatology, Palaeoecology*, **295**, 102–115, https://doi.org/10.1016/j.palaeo.2010.05.021

Cohen, A.S., Coe, A.L., Harding, S.M. and Schark, L. 2004. Osmium isotope evidence for the regulation of atmospheric CO_2 by continental weathering. *Geology*, **32**, 157–160, https://doi.org/10.1130/G20158.1

Cope, J.C.W., Ingham, J.K. and Rawson, P.F. 1992. *Atlas of Palaeogeography and Lithofacies*. Geological Society, London, Memoirs, **13**.

Copestake, P. and Johnson, B. 2014. *Lower Jurassic Foraminifera from the Llanbedr (Mochras Farm) Borehole, North Wales, UK*. Palaeontographical Society, Monographs, **641**.

Curtis, C.D. and Spears, D.A. 1968. The formation of sedimentary iron minerals. *Economic Geology*, **63**, 257–270, https://doi.org/10.2113/gsecongeo.63.3.257

Deconinck, J.-F., Hesselbo, S.P. and Pellenard, P. 2019. Climatic and sea-level control of Jurassic (Pliensbachian) clay mineral sedimentation in the Cardigan Bay Basin, Llanbedr (Mochras Farm) borehole, Wales. *Sedimentology*, **66**, 2769–2783, https://doi.org/10.1111/sed.12610

Deconinck, J.-F., Gómez, J.J. *et al.* 2020. Diagenetic and environmental control of the clay mineralogy, organic matter and stable isotopes (C, O) of Jurassic (Pliensbachian–lowermost Toarcian) sediments of the Rodiles section

(Asturian Basin, northern Spain). *Marine and Petroleum Geology*, **115**, 104286, https://doi.org/10.1016/j.marpetgeo.2020.104286

Dera, G. and Donnadieu, Y. 2012. Modeling evidence for global warming, Arctic seawater freshening, and sluggish oceanic circulation during the Early Toarcian anoxic event. *Paleoceanography*, **27**, PA2211, https://doi.org/10.1029/2012PA002283

Dera, G., Pellenard, P., Neige, P., Deconinck, J.-F., Pucéat, E. and Dommergues, J.-L. 2009. Distribution of clay minerals in Early Jurassic Peritethyan seas: paleoclimatic significance inferred from multiproxy comparisons. *Palaeogeography, Palaeoclimatology, Palaeoecology*, **271**, 39–51, https://doi.org/10.1016/j.palaeo.2008.09.010

Dera, G., Brigaud, B. *et al.* 2011. Climatic ups and downs in a disturbed Jurassic world. *Geology*, **39**, 215–218, https://doi.org/10.1130/G31579.1

Dickson, J.A.D. 2001. Diagenesis and crystal caskets: echinoderm Mg calcite transformation, Dry Canyon, New Mexico, USA. *Journal of Sedimentary Research*, **71**, 764–777, https://doi.org/10.1306/2DC40966-0E47-11D7-8643000102C1865D

Dobson, M.R. and Whittington, R.J., 1987. The geology of Cardigan Bay. *Proceedings of the Geologists' Association*, **98**, 331–353, https://doi.org/10.1016/S0016-7878(87)80074-3

Duarte, L.V., Comas-Rengifo, M.J., Silva, R.L., Paredes, R. and Goy, A. 2014. Carbon isotope stratigraphy and ammonite biochronostratigraphy across the Sinemurian–Pliensbachian boundary in the western Iberian margin. *Bulletin of Geosciences*, **89**, 719–736, https://doi.org/10.3140/bull.geosci.1476

Fantasia, A., Föllmi, K.B., Adatte, T., Spangenberg, J.E. and Montero-Serrano, J.-C. 2018. The Early Toarcian oceanic anoxic event: paleoenvironmental and paleoclimatic change across the Alpine Tethys (Switzerland). *Global and Planetary Change*, **162**, 53–68, https://doi.org/10.1016/j.gloplacha.2018.01.008

Fantasia, A., Adatte, T., Spangenberg, J.E., Font, E., Duarte, L.V. and Föllmi, K.B. 2019. Global versus local processes during the Pliensbachian–Toarcian transition at the Peniche GSSP, Portugal: a multi-proxy record. *Earth-Science Reviews*, **198**, 102932, https://doi.org/10.1016/j.earscirev.2019.102932

Ferreira, J., Mattioli, E. *et al.* 2019. Western Tethys Early and Middle Jurassic calcareous nannofossil biostratigraphy. *Earth-Science Reviews*, **197**, 102908, https://doi.org/10.1016/j.earscirev.2019.102908

Gómez, J.J., Goy, A. and Canales, M.L. 2008. Seawater temperature and carbon isotope variations in belemnites linked to mass extinction during the Toarcian (Early Jurassic) in Central and Northern Spain. Comparison with other European sections. *Palaeogeography, Palaeoclimatology, Palaeoecology*, **258**, 28–58, https://doi.org/10.1016/j.palaeo.2007.11.005

Gorzelak, P., Krzykawski, T. and Stolarski, J. 2016. Diagenesis of echinoderm skeletons: constraints on paleoseawater Mg/Ca reconstructions. *Global and Planetary Change*, **144**, 142–157, https://doi.org/10.1016/j.gloplacha.2016.07.010

Hałas, S. and Chlebowski, R. 2004. Unique siderite occurrence in Baltic Sea: a clue to siderite–water oxygen isotope fractionation at low temperatures. *Geological Quarterly*, **48**, 317–322.

Haq, B.U. 2018. Jurassic sea-level variations: a reappraisal. *GSA Today*, **28**, 4–10, https://doi.org/10.1130/GSATG359A.1

Hermoso, M., Minoletti, F., Rickaby, R.E.M., Hesselbo, S.P., Baudin, F. and Jenkyns, H.C. 2012. Dynamics of a stepped carbon-isotope excursion: ultra high-resolution study of Early Toarcian environmental change. *Earth and Planetary Science Letters*, **319–320**, 45–54, https://doi.org/10.1016/j.epsl.2011.12.021

Hesselbo, S.P. 2008. Sequence stratigraphy and inferred relative sea-level change from the onshore British Jurassic. *Proceedings of the Geologists' Association*, **119**, 19–34, https://doi.org/10.1016/S0016-7878(59)80069-9

Hesselbo, S.P., Gröcke, D.R., Jenkyns, H.C., Bjerrum, C.J., Farrimond, P., Morgans Bell, H.S. and Green O.R. 2000. Massive dissociation of gas hydrate during a Jurassic oceanic anoxic event. *Nature*, **406**, 392–395, https://doi.org/10.1038/35019044

Hesselbo, S.P., Robinson, S.A., Surlyk, F. and Piasecki, S. 2002. Terrestrial and marine extinction at the Triassic–Jurassic boundary synchronized with major carbon-cycle perturbation: a link to initiation of massive volcanism? *Geology*, **30**, 251–254, https://doi.org/10.1130/0091-7613(2002)030<0251:TAMEAT>2.0.CO;2

Hesselbo, S.P., Jenkyns, H.C., Duarte, L.V. and Oliveira, L.C.V. 2007. Carbon-isotope record of the Early Jurassic (Toarcian) oceanic anoxic event from fossil wood and marine carbonate (Lusitanian Basin, Portugal). *Earth and Planetary Science Letters*, **253**, 455–470, https://doi.org/10.1016/j.epsl.2006.11.009

Hesselbo, S.P., Ogg, J.G., Ruhl, M., Hinnov, L.A. and Huang, C.J. 2020*a*. The Jurassic Period. *In*: Gradstein, F.M., Ogg, J.G., Schmitz, M.D. and Ogg, G.M. (eds) *Geologic Time Scale 2020*. Elsevier, 955–1021.

Hesselbo, S.P., Hudson, A.J.L., Huggett, J.M., Leng, M.J., Riding, J.B. and Ullmann, C.V. 2020*b*. Palynological, geochemical, and mineralogical characteristics of the Early Jurassic Liasidium event in the Cleveland Basin, Yorkshire, UK. *Newsletters on Stratigraphy*, **53**, 191–211, https://doi.org/10.1127/nos/2019/0536

Hesselbo, S.P., Korte, C., Ullmann, C.V. and Ebbesen, A.L. 2020*c*. Carbon and oxygen isotope records from the southern Eurasian Seaway following the Triassic–Jurassic boundary: parallel long-term enhanced carbon burial and seawater warming. *Earth-Science Reviews*, **203**, 103131, https://doi.org/10.1016/j.earscirev.2020.103131

Hoareau, G., Monnin, C. and Odonne, F. 2010. A study of celestine equilibrium in marine sediments using the entire ODP/IODP porewater data base. *Geochimica et Cosmochimica Acta*, **74**, 3925–3937, https://doi.org/10.1016/j.gca.2010.03.033

Holford, S.P., Green, P.F. and Turner, J.P. 2005. Paleothermal and compaction studies in the Mochras borehole (NW Wales) reveal early Cretaceous and Neogene exhumation and argue against regional Palaeogene uplift in the southern Irish Sea. *Journal of the Geological Society, London*, **162**, 829–840, https://doi.org/10.1144/0016-764904-118

Huggett, J., Dennis, P. and Gale, A. 2000. Geochemistry of early siderite cements from the Eocene succession of Whitecliff Bay, Hampshire Basin, UK. *Journal of Sedimentary Research*, **70**, 1107–1117, https://doi.org/10.1306/112399701107

Irwin, H., Curtis, C. and Coleman, M. 1977. Isotopic evidence for source of diagenetic carbonates formed during burial of organic-rich sediments. *Nature*, **269**, 209–213, https://doi.org/10.1038/269209a0

Jenkyns, H.C. and Clayton, C.J. 1986. Black shales and carbon isotopes in pelagic sediments from the Tethyan Lower Jurassic. *Sedimentology*, **33**, 87–106, https://doi.org/10.1111/j.1365-3091.1986.tb00746.x

Jenkyns, H.C., Jones, C.E., Gröcke, D.R., Hesselbo, S.P. and Parkinson, D.N. 2002. Chemostratigraphy of the Jurassic System: applications, limitations and implications for palaeoceanography. *Journal of the Geological Society, London*, **159**, 351–378, https://doi.org/10.1144/0016-764901-130

Jones, C.E., Jenkyns, H.C. and Hesselbo, S.P. 1994. Strontium isotopes in Early Jurassic seawater. *Geochimica et Cosmochimica Acta*, **58**, 1285–1301, https://doi.org/10.1016/0016-7037(94)90179-1

Katz, M.E., Wright, J.D., Miller, K.G., Cramer, B.S., Fennel, K. and Falkowski, P.G. 2005. Biological overprint of the geological carbon cycle. *Marine Geology*, **217**, 323–338, https://doi.org/10.1016/j.margeo.2004.08.005

Kemp, D.B., Coe, A.L., Cohen, A.S. and Schwark, L. 2005. Astronomical pacing of methane release in the Early Jurassic period. *Nature*, **437**, 396–399, https://doi.org/10.1038/nature04037

Korte, C. and Hesselbo, S.P. 2011. Shallow marine carbon and oxygen isotope and elemental records indicate icehouse–greenhouse cycles during the Early Jurassic. *Paleoceanography*, **26**, PA4219, https://doi.org/10.1029/2011PA002160

Korte, C., Hesselbo, S.P., Jenkyns, H.C., Rickaby, R.E.M. and Spötl, C. 2009. Palaeoenvironmental significance of carbon- and oxygen-isotope stratigraphy of marine Triassic–Jurassic boundary sections in SW Britain. *Journal of the Geological Society, London*, **166**, 431–445, https://doi.org/10.1144/0016-76492007-177

Korte, C., Hesselbo, S.P., Ullmann, C.V., Dietl, G., Ruhl, M., Schweigert, G. and Thibault, N. 2015. Jurassic climate mode governed by ocean gateway. *Nature Communications*, **6**, 10015, https://doi.org/10.1038/ncomms10015

Littler, K., Hesselbo, S.P. and Jenkyns, H.C. 2010. A carbon-isotope perturbation at the Pliensbachian–Toarcian boundary: evidence from the Lias Group, NE England. *Geological Magazine*, **147**, 181–192, https://doi.org/10.1017/S0016756809990458

Lohmann, K.C. 1983. *AAPG Short Course:* Unravelling the Diagenetic History of Carbonate Reservoirs: Integration of Petrographic and Geochemical Techniques. *Presented at Section V, Dallas, TX, USA*.

McArthur, J.M., Donovan, D.T., Thirlwall, M.F., Fouke, B.W. and Mattey, D. 2000. Strontium isotope profile of the early Toarcian (Jurassic) oceanic anoxic event, the duration of ammonite biozones, and belemnite palaeotemperatures. *Earth and Planetary Science Letters*, **179**, 269–285, https://doi.org/10.1016/S0012-821X(00)00111-4

McArthur, J.M., Algeo, T.J., van de Schootbrugge, B., Li, Q. and Howarth, R.J. 2008. Basinal restriction, black shales, Re–Os dating, and the Early Toarcian (Jurassic) oceanic anoxic event. *Paleoceanography*, **23**, PA4217, https://doi.org/10.1029/2008PA001607

Mercuzot, M., Pellenard, P. *et al.* 2020. Carbon-isotope events during the Pliensbachian (Lower Jurassic) on the African and European margins of the NW Tethyan Realm. *Newsletters on Stratigraphy*, **53**, 41–69, https://doi.org/10.1127/nos/2019/0502

Mortimer, R.J. and Coleman, M.L. 1997. Microbial influence on the oxygen isotopic composition of diagenetic siderite. *Geochimica et Cosmochimica Acta*, **61**, 1705–1711, https://doi.org/10.1016/S0016-7037(97)00027-6

Munier, T., Deconinck, J.-F. *et al.* 2020. Million-year-scale alternation of warm-humid and semi-arid periods as a mid-latitude climate mode in the Early Jurasic (Late Sinemurian, Laurasian Seaway) [preprint] *Climate of the Past Discussion*, https://doi.org/10.5194/cp-2020-99 [last accessed 21 June 2021]

Okita, P.M., Maynard, J.B., Spiker, E.C. and Force, E.R. 1988. Isotopic evidence for organic matter oxidation by manganese reduction in the formation of stratiform manganese carbonate ore. *Geochimica et Cosmochimica Acta*, **52**, 2679–2685, https://doi.org/10.1016/0016-7037(88)90036-1

Pearson, M.J. and Nelson, C.S. 2005. Organic geochemistry and stable isotope composition of New Zealand carbonate concretions and calcite fracture fills. *New Zealand Journal of Geology and Geophysics*, **48**, 395–414, https://doi.org/10.1080/00288306.2005.9515122

Percival, L.M., Cohen, A.S. *et al.* 2016. Osmium isotope evidence for two pulses of increased continental weathering linked to Early Jurassic volcanism and climate change. *Geology*, **44**, 759–762, https://doi.org/10.1130/G37997.1

Peti, L., Thibault, N. *et al.* 2017. Sinemurian–Pliensbachian calcareous nannofossil biostratigraphy and organic carbon isotope stratigraphy in the Paris Basin: calibration to the ammonite biozonation of NW Europe.

Palaeogeography, Palaeoclimatology, Palaeoecology, **468**, 142–161, https://doi.org/10.1016/j.palaeo.2016.12.004

Price, G.D., Baker, S.J., VanDeVelde, J. and Clémence, M.-E. 2016. High-resolution carbon cycle and seawater temperature evolution during the Early Jurassic (Sinemurian–Early Pliensbachian). *Geochemistry, Geophysics, Geosystems*, **17**, 3917–3928, https://doi.org/10.1002/2016GC006541

Riding, J.B., Leng, M.J., Kender, S., Hesselbo, S.P. and Feist-Burkhardt, S. 2013. Isotopic and palynological evidence for a new Early Jurassic environmental perturbation. *Palaeogeography, Palaeoclimatology, Palaeoecology*, **374**, 16–27, https://doi.org/10.1016/j.palaeo.2012.10.019

Rita, P., Nätscher, P., Duarte, L.V., Weis, R. and De Baets, K. 2019. Mechanisms and drivers of belemnite body-size dynamics across the Pliensbachian–Toarcian crisis. *Royal Society Open Science*, **6**, 190494, https://doi.org/10.1098/rsos.190494

Rosales, I., Robles, S. and Quesada, S. 2004. Elemental and oxygen isotope composition of Early Jurassic belemnites: salinity vs. temperature signals. *Journal of Sedimentary Research*, **74**, 342–354, https://doi.org/10.1306/112603740342

Ruebsam, W. and Al-Husseini, M. 2020. Calibrating the Early Toarcian (Early Jurassic) with stratigraphic black holes (SBH). *Gondwana Research*, **82**, 317–336, https://doi.org/10.1016/j.gr.2020.01.011

Ruhl, M., Kürschner, W.M. and Krystyn, L. 2009. Triassic–Jurassic organic carbon isotope stratigraphy of key sections in the western Tethys realm (Austria). *Earth and Planetary Science Letters*, **281**, 169–187, https://doi.org/10.1016/j.epsl.2009.02.020

Ruhl, M., Deenen, M.H.L., Abels, H.A., Bonis, N.R., Krijgsman, W. and Kürschner, W.M. 2010. Astronomical constraints on the duration of the early Jurassic Hettangian stage and recovery rates following the end-Triassic mass extinction (St Audrie's Bay/East Quantoxhead, UK). *Earth and Planetary Science Letters*, **295**, 262–276, https://doi.org/10.1016/j.epsl.2010.04.008

Ruhl, M., Hesselbo, S.P. *et al.* 2016. Astronomical constraints on the duration of the Early Jurassic Pliensbachian Stage and global climatic fluctuations. *Earth and Planetary Science Letters*, **455**, 149–165, https://doi.org/10.1016/j.epsl.2016.08.038

Saelen, G and Karstang, T.V. 1989. Chemical signatures of belemnites. *Neues Jahrbuch für Geologie und Paläontologie Abhandlung*, **177**, 333–346.

Saelen, G., Doyle, P. and Talbot, M.R. 1996. Stable-isotope analyses of belemnite rostra from the Whitby Mudstone Fm., England: surface water conditions during deposition of a marine black shale. *Palaios*, **11**, 97–117, https://doi.org/10.2307/3515065

Schöllhorn, I., Adatte, T., van de Schootbrugge, B., Houben, A., Charbonnier, G., Janssen, N. and Föllmi, K.B. 2020. Climate and environmental response to the break-up of Pangea during the Early Jurassic (Hettangian–Pliensbachian); the Dorset coast (UK) revisited. *Global and Planetary Change*, **185**, 103096, https://doi.org/10.1016/j.gloplacha.2019.103096

Sheppard, T.H., Houghton, R.D. and Swan, A.R.H. 2006. Bedding and pseudo-bedding in the Early Jurassic of Glamorgan: deposition and diagenesis of the Blue Lias in South Wales. *Proceedings of the Geologists' Association*, **117**, 249–264, https://doi.org/10.1016/S0016-7878(06)80033-7

Storm, M.S., Hesselbo, S.P. *et al.* 2020. Orbital pacing and secular evolution of the Early Jurassic carbon cycle. *PNAS*, **117**, 3974–3982, https://doi.org/10.1073/pnas.1912094117

Suan, G., Mattioli, E., Pittet, B., Mailliot, S. and Lécuyer, C. 2008. Evidence for major environmental perturbation prior to and during the Toarcian (Early Jurassic) oceanic anoxic event from the Lusitanian Basin, Portugal. *Paleoceanography*, **23**, PA1202, https://doi.org/10.1029/2007PA001459

Swart, P.K. 2015. The geochemistry of carbonate diagenesis: the past, present and future. *Sedimentology*, **62**, 1233–1304, https://doi.org/10.1111/sed.12205

Tappin, D.R., Chadwick, R.A., Jackson, A.A., Wingfield, R.T.R. and Smith, N.J.P. 1994. *The Geology of Cardigan Bay and the Bristol Channel*. *British Geological Survey, Offshore Regional Report.*

Ullmann, C.V. and Korte, C. 2015. Diagenetic alteration in low-Mg calcite from macrofossils: a review. *Geological Quarterly*, **59**, 3–20, https://doi.org/10.7306/gq.1217

Ullmann, C.V., Campbell, H.J., Frei, R., Hesselbo, S.P., Pogge von Strandmann, P.A.E. and Korte, C. 2013. Partial diagenetic overprint of Late Jurassic belemnites from New Zealand: implications for the preservation potential of δ^7Li values in calcite fossils. *Geochimica et Cosmochimica Acta*, **120**, 80–96, https://doi.org/10.1016/j.gca.2013.06.029

Ullmann, C.V., Thibault, N., Ruhl, M., Hesselbo, S.P. and Korte, C. 2014. Effect of a Jurassic oceanic anoxic event on belemnite ecology and evolution. *PNAS*, **111**, 10073–10076, https://doi.org/10.1073/pnas.1320156111

Ullmann, C.V., Frei, R., Korte, C. and Hesselbo, S.P. 2015. Chemical and isotopic architecture of the belemnite rostrum. *Geochimica et Cosmochimica Acta*, **159**, 231–243, https://doi.org/10.1016/j.gca.2015.03.034

Ullmann, C.V., Frei, R., Korte, C. and Lüter, C. 2017. Element/Ca, C and O isotope ratios in modern brachiopods: species-specific signals of biomineralisation. *Chemical Geology*, **460**, 15–24, https://doi.org/10.1016/j.chemgeo.2017.03.034

Ullmann, C.V., Boyle, R. *et al.* 2020. Warm afterglow from the Toarcian oceanic anoxic event drives the success of deep-adapted brachiopods. *Scientific Reports*, **10**, 6549, https://doi.org/10.1038/s41598-020-61393-5

van de Schootbrugge, B., Bailey, T.R. *et al.* 2005*a*. Early Jurassic climate change and the radiation of organic-walled phytoplankton in the Tethys Ocean. *Paleobiology*, **31**, 73–97, https://doi.org/10.1666/0094-8373(2005)031<0073:EJCCAT>2.0.CO;2

van de Schootbrugge, B., McArthur, J.M., Bailey, T.R., Rosenthal, Y., Wright, J.D. and Miller, K.G. 2005*b*. Toarcian oceanic anoxic event: an assessment of global causes using belemnite C isotope records. *Paleoceanography*, **20**, PA3008, https://doi.org/10.1029/2004PA001102

van de Schootbrugge, B., Harazim, D. *et al.* 2010. The enigmatic ichnofossil *Tisoa siphonalis* and widespread authigenic seep carbonate formation during the Late Pliensbachian in southern France. *Biogeosciences*, **7**, 3123–3138, https://doi.org/10.5194/bg-7-3123-2010

Voigt, S., Wilmsen, M., Mortimore, R.N. and Voigt, T. 2003. Cenomanian palaeotemperatures derived from the oxygen isotopic composition of brachiopods and belemnites: evaluation of Cretaceous palaeotemperature proxies. *International Journal of Earth Sciences*, **92**, 285–299, https://doi.org/10.1007/s00531-003-0315-1

Weedon, G.P. 1986. Hemipelagic shelf sedimentation and climatic cycles: the basal Jurassic (Blue Lias) of South Britain. *Earth and Planetary Science Letters*, **76**, 321–335, https://doi.org/10.1016/0012-821X(86)90083-X

Weedon, G.P., Jenkyns, H.C. and Page, K. 2018. Combined sea-level and climate controls on limestone formation, hiatuses and ammonite preservation in the Blue Lias Formation, south Britain (uppermost Triassic–Lower Jurassic). *Geological Magazine*, **155**, 1117–1148, https://doi.org/10.1017/S001675681600128X

Weissert, H., McKenzie, J. and Hochuli, P. 1979. Cyclic anoxic events in the Early Cretaceous Tethys Ocean. *Geology*, **7**, 147–151, https://doi.org/10.1130/0091-7613(1979)7<147:CAEITE>2.0.CO;2

Wood, A. and Woodland, A.W. 1968. Borehole at Mochras, West of Llanbedr, Merionethshire. *Science*, **219**, 1352–1354.

Woodland, A.W. (ed.) 1971. *The Llanbedr-Mochras Farm-Borehole*. HMSO.

Xu, W., Ruhl, M. *et al.* 2018*a*. Evolution of the Toarcian (Early Jurassic) carbon-cycle and global climatic controls on local sedimentary processes (Cardigan Bay Basin, UK). *Earth and Planetary Science Letters*, **484**, 396–411, https://doi.org/10.1016/j.epsl.2017.12.037

Xu, W., Mac Niocaill, C., Ruhl, M., Jenkyns, H.C., Riding, J.B. and Hesselbo, S.P. 2018*b*. Magnetostratigraphy of the Toarcian Stage (Lower Jurassic) of the Llanbedr (Mochras Farm) Borehole, Wales: basis for a global standard and implications for volcanic forcing of palaeoenvironmental change. *Journal of the Geological Society, London*, **175**, 594–604, https://doi.org/10.1144/jgs2017-120